

Experimental study on square RC short columns strengthened with corrugated steel jacket under axial compression

Yang Fan^a, Yang Ligui^{*b}, Wang Yuyin^{c,d}, Fang Yong^{c,d}, Jin Shuangshuang^b, Chen Yunwen^b, Xia Qilong^a

^a No.3 Construction Co., Ltd. of Chongqing Construction Engineering Group;

^b School of Civil Engineering, Chongqing Jiaotong University, Chongqing 400074, China;

^c Key Lab of Structures Dynamic Behaviour and Control of the Ministry of Education, Harbin Institute of Technology, Harbin150090, China;

^d School of Civil Engineering, Harbin Institute of Technology, Heilongjiang, Harbin150090, China

Abstract: In the long-term service of life, structural columns may experience mechanical performance degradation due to environmental erosion, various hazards, and functional modifications. This study proposes a novel concrete column reinforcement method utilizing square corrugated steel jackets as external confinement components, which significantly enhances both bearing capacity and ductility of original members. To investigate the mechanical performance improvement mechanisms and load-carry mode, 10 axially compressed short column specimens were designed. Detailed analyses were conducted surrounding the effects of connection methods for corrugated sheets, corrugated steel thickness, and damage levels on load-displacement curves, as well as stress and strain development patterns. A computational model for ultimate bearing capacity of reinforced sections was established. Key findings include: (1) The use of corrugated steel sleeves can enhance the ultimate bearing capacity of the original short columns by 34.6% to 67.3%. (2) Considering that the confinement effect of square sleeves is not optimal, it is more material-efficient to use thinner corrugated steel plates to achieve similar results. (3) There is no significant difference in the effects of connection types on mechanical performance. (4) The cracking and softening of damaged concrete can enhance the confinement effect in corrugated steel-strengthened reinforced concrete columns. (5) The confined concrete strength model can be used to accurately predict the ultimate bearing capacity.

Keywords: Concrete-filled corrugated steel tube (CFCST), corrugated steel sheet, confined concrete, axial compression, ultimate load-bearing capacity.

1 Introduction

The safety and durability of buildings during urbanization are critical factors for modern construction [1]. Throughout their service life, structural systems inevitably experience damage or even collapse due to the influence of natural factors such as wind disasters, floods, fires, earthquakes, and other extreme events, as well as human-induced impacts [2]-[5] (as illustrated in Fig. 1). These challenges pose significant risks to urban development. Given the growing complexity of building systems, ensuring long-term safety and durability has become an increasingly pressing issue [6]. In recent years, many aged structures have already exhibited performance impairments due to the progressive degradation of their load-carrying capacity and ductility. Such impairments can lead to reduced serviceability and increased vulnerability to failure events. In modern urban renewal efforts, faced with aged structures that have not yet met demolition standards, demolishing and rebuilding requires substantial economic investment while generating massive construction waste, causing environmental pollution, and wasting valuable human resources and time. A large number of buildings constructed in the 20th century are currently entering a stage requiring urgent reinforcement and retrofitting [7]. Simultaneously, many culturally significant heritage buildings also demand ongoing daily maintenance and preservation [8]. Therefore, repairing, reinforcing, or retrofitting damaged existing structures is often an ideal choice, which combines economic efficiency with long-term benefits in terms of structural performance and sustainability.

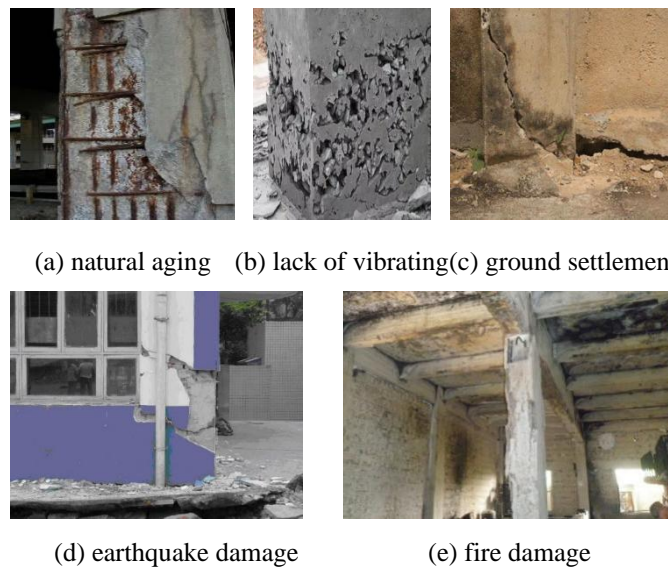


Fig. 1. Damage and failure of column

Columns serve as the most critical vertical load-bearing components in buildings, and their

effective load carrying is particularly important for ensuring the overall structural safety of a building. The low-story columns of high-rise buildings, due to their relatively larger axial compression ratio, are more susceptible to damage if their bearing capacity becomes insufficient[11]. This can lead to significant safety risks. Various structural reinforcement methods for reinforced concrete columns, as shown in **Fig. 2**, have been proposed to address these issues, including: enlarging section using concrete [12]-[16], Strengthening using steel angles and strips[17],[18], jacketing with steel sheets[19]-[21].

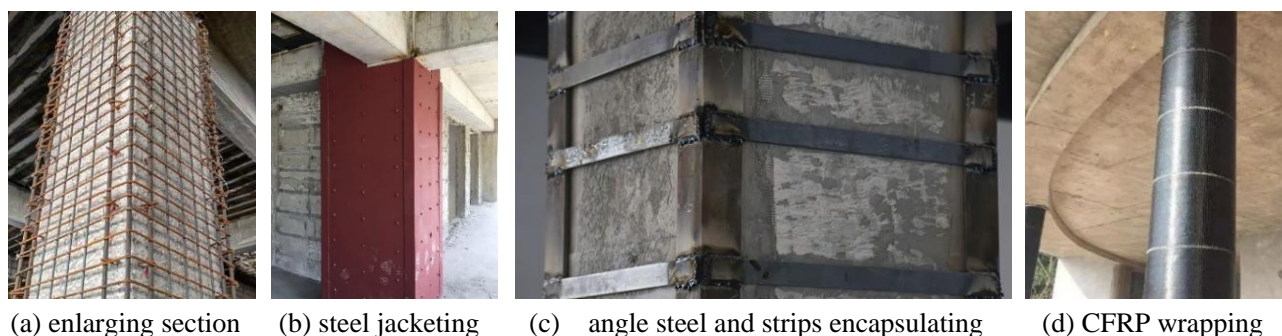


Fig.2. Typical strengthening method of column.

In recent years, more methods have been developed to strengthen reinforced concrete columns using novel high-strength materials, such as glass-fiber reinforced plastic (GFRP) tubes, ultra-high-performance concrete (UHPC), carbon fiber-reinforced columns, and concrete columns wrapped with CFRP strips or fabrics [22]-[31]. Ghobarah and Bidda (1997) [32][33] proposed a method of reinforcing beams and columns using corrugated steel sleeves. As shown in Fig. 3, the corrugated steel sheets are assembled into sleeves to encase the damaged column ends and beam-column joints after an earthquake, which is similar to Tommi's earlier proposal for corrugated steel tube columns [34]. The externally applied corrugated steel jackets significantly increase the load-bearing capacity of the columns due to their circumferential confinement to the core concrete. Yang et al. (2020) [35] investigated the compressive behaviour of the concrete-filled corrugated steel tubular columns, and found that even with thin walls, corrugated steel can provide excellent circumferential confinement to the core component.

Considering the mechanical advantages, concrete columns strengthened with a corrugated steel jacket may exhibit good mechanical performance due to the combined benefits of the jacket's encasement and the corrugations' interlocking effect [36]. The jacket also prevents secondary cracking or spalling of the repair layer during service, thereby eliminating the need for frequent inspections. In

addition, retrofitting existing reinforced concrete columns with galvanized corrugated steel provides excellent corrosion resistance due to the protective zinc coating and dense oxide film on the surface of the galvanized steel [37]. This results in both maintenance-free service performance and reduced management/maintenance costs. The corrugated steel jacket can serve as formwork due to its significant transverse stiffness. Compared to conventional steel plate reinforcement, this method reduces structural steel usage and minimizes on-site welding operations.

A composite member can be obtained by using corrugated steel plates or tubes to enhance a reinforced concrete (RC) column. For similar concrete columns, Fang et. al. [38][39] investigated the load-bearing capacity of circular-section galvanized corrugated steel tube infilled with concrete (CFDST) and built a design approach for such a novel composite column. For concrete-filled square corrugated steel tubular columns, Zou Y. [40], Yu C. [41], and Nassirnia M. [42] conducted compression and eccentric compression tests, demonstrating that the sleeve method effectively constrains the core concrete. They explained, from a theoretical perspective, why corrugated steel sleeves can significantly restore and enhance the mechanical performance of concrete. Lu and Fang et al. (2024) [43] studied the hysteresis performance of concrete-filled double-skin corrugated steel tubes under combined compression and cyclic lateral loads, revealing that the confinement effect of the corrugated steel tube plays a critical role in improving the ductility of the column. They also proposed design formulas for the compression-bending combined resistance of such a hollow-section member. Handousa A. and Abdellatif M. et al. (2025) [44] employed two machine learning models to predict the ultimate load-bearing capacity of concrete-filled corrugated steel tubular columns: Artificial Neural Network (ANN) and Gaussian Process Regression (GPR).

As the structural enhancement mechanisms of corrugated steel to the damaged concrete is overlooked in existing studies, this investigation examines the corrugated steel jacketing the concrete column with damage through comprehensive experimental and analytical approaches. Ten short-column specimens were fabricated and subjected to axial compression testing, with particular emphasis on elucidating failure patterns, and ultimate load characteristics. A parametric test was systematically conducted, incorporating three primary variables: connection configuration, corrugated steel plate thickness (ranging 1.6-2.7 mm), and initial damage severity (quantified by 40-100% initial compression ratio). Throughout experimental procedures, the strain evolution in the corrugated steel

jackets was continuously monitored, and complemented by elastoplastic analysis to characterize stress redistribution phenomena. The study clarifies the composite action mechanism whereby the confinement from corrugated steel effectively enhances the residual capacity of the damaged concrete core through triaxial compression. Building upon the established ultimate state model of axially compressed sections, a novel theoretical method was developed incorporating confinement and damage reduction factors, enabling precise prediction of retrofitted RC columns' load-bearing capacity with less than 1.86% deviation from experimental values. Calculation methods recommended by the existing codes were modified for such a strengthened cross section. From the systematically comparison results, a simple calculation formula was suggested in the application.

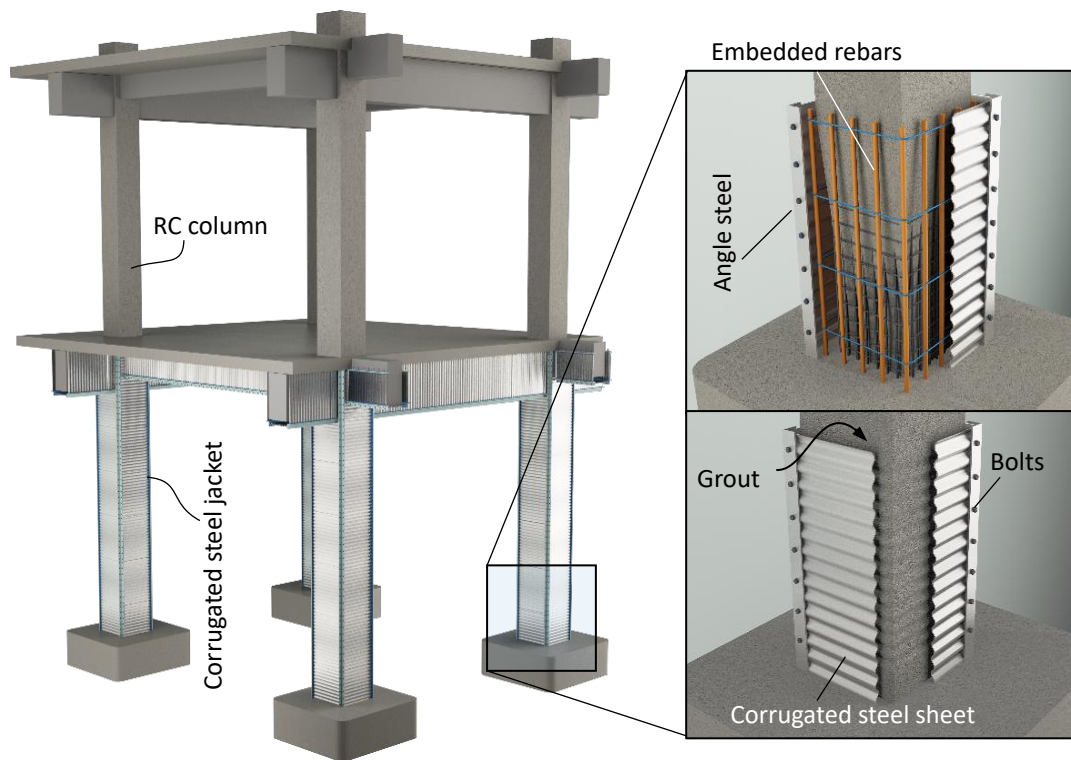


Fig. 3. Diagram of strengthening RC columns by corrugated steel jacket.

2 Experimental arrangements

2.1 Specimens parameters

As illustrated in **Table 1**, ten specimens were designed to observe the confinement effect of corrugated steel jacket to the concrete. To quantitatively compare the enhancement in load-bearing capacity, there is one reinforced concrete (RC) short column directly compressed to be crushed. The original RC parts of all specimens are fabricated with the same reinforcement ratio (longitudinal bars

ratio=1.1%, and stirrups ratio=0.5%). The corrugated steel plates are formed by bending Q355 steel plates, and the corrugation profile length×height is 68×13 mm×mm. The reinforcement layer is filled with grout, filling gap of 14-22mm according to measurement.

Table 1. Parameters of specimens

No.	Specimens	t_{cs} (mm)	t_g (mm)	B (mm)	L (mm)	σ_0	f_c^i (MPa)	N_u (kN)	Connection type
1	RC	/	/	200×200	748	/	44.5	2117.7	/
2	CS-A-2-0.4	2.0	14.0	241×241	748	$0.4f_c$	44.5	2957.4	Connection A
3	CS-B-2-0.4	2.0	21.5	256×256	748	$0.4f_c$	44.5	3101.1	Connection B
4	CS-C-2-0.4	2.0	17.0	247×247	748	$0.4f_c$	44.5	3125.6	Connection C
5	CS-D-1.6-0.4	1.6	22.0	257×257	748	$0.4f_c$	54.9	3361.3	Connection D
6	CS-D-2.7-0.4	2.7	22.0	257×257	748	$0.4f_c$	54.9	3314.0	Connection D
7	CS-D-2-0.4	2.0	22.0	257×257	748	$0.4f_c$	54.9	3543.4	Connection D
8	CS-D-2-0.6a	2.0	22.0	257×257	748	$0.6f_c$	54.9	3365.8	Connection D
9	CS-D-2-0.6b	2.0	22.0	257×257	748	$0.6f_c$	54.9	3412.9	Connection D
10	CS-D-2-1.0	2.0	22.0	257×257	748	$1.0f_c$	44.5	2850.9	Connection D

Notes: “CS” represents the corrugated steel plate reinforced specimen; “A” indicates that the corner the corrugated steel is connected with angle steel and flange plate bolted connection; “B” indicates that the corrugated steel is connected by bolts along with the vertical line in the middle of the specimen; “C” indicates that the corner connection of the corrugated steel is bolted with a special-shaped steel; “D” indicates that the corrugated steel and angle steel are fully welded. For example, **CS-A-2-0.4** means that the corner connection of the corrugated steel is the type-A, the corrugated steel wall thickness is 2 mm, and the initial damage stress reaches $0.4f_c$.

The specimen is designed with three influencing factors, namely the corner connection type, corrugated steel thickness, and the degree of concrete initial stress. The corrugated steel sleeve of the specimen is made by splicing several corrugated steel sheets. To ensure the effectiveness of the connection configurations for the corrugated steel, four different connection types of the corrugated steel plates were compared, as shown in **Fig. 4**.

(1) **Connection-A**: Angle steel is welded to the corrugated steel plate, and two L-shaped units are bolted together at the corner to form the sleeve.

(2) **Connection-B**: The corrugated steel plates are pre-welded into U-shaped units using angle steel, and then two U-shaped units are connected into a sleeve using a group of bolts.

(3) **Connection-C**: Similar to Connection-A, but the angle steel is replaced with a τ -shaped special connector to increase the flow space for grouting at the corner.

(4) **Connection-D:** Each corrugated steel plate is directly welded to the angle steel in the corner.

The corrugated steel plates of the specimen are designed with three wall thicknesses: 1.6 mm, 2.0 mm, and 2.7 mm, to study the effect of corrugated steel wall thickness on the mechanical properties of reinforced concrete columns strengthened with corrugated steel sleeves. To investigate the impact of different damage levels on the load-carrying capacity enhancement, specimens with initial axial compression ratios of $\sigma_0/f_c=0.4, 0.6,$ and 1.0 (i.e., on ultimate state) were also set up for reinforcement.

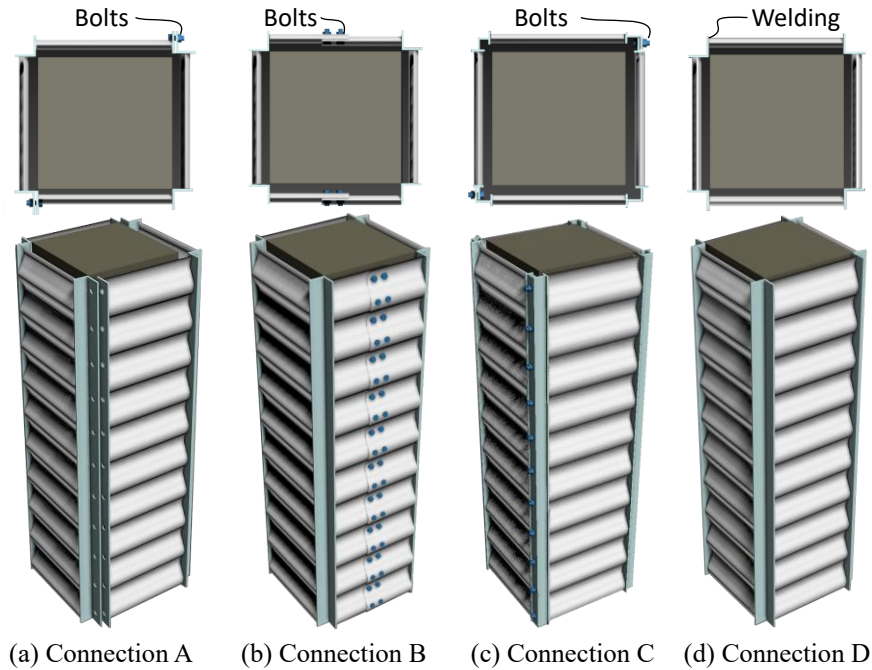


Fig. 4 Connection types.

2.2 Arrangement of specimens

The workflow of fabrication process of axially compressed short columns and strengthening specimens includes: reinforcement cage fabrication, concrete pouring and curing, angle steel welding, corrugated steel plate cutting and welding, strengthening jacket fabrication, damage applying, sleeve enclosure, and interlayer grout pouring.

Based on the initial axial compression ratio designed in Table 1, varying magnitudes of axial pressure are applied to reinforced concrete short columns to replicate the stress states of actual structural columns. Subsequently, the pressure is unloaded to zero to simulate the vertical support removal effect in strengthening structures. Following **Fig. 4** specifications, a connection sleeve is fabricated and installed around the damaged reinforced concrete specimen. Grout is then poured into the interlayer between the concrete and corrugated steel plates. To ensure full filling of the corrugated

steel-concrete interlayer, a two-stage pouring process is adopted:

(1) First-stage pouring: As shown in **Fig.5**, the column is vertically positioned on the ground. Grout is poured from top to bottom through gaps near the upper end and vibrated to ensure compaction. After initial setting of the first-stage grout (cured for one day),

(2) Second-stage pouring: The specimen is laid horizontally for secondary pouring. Steel plates are welded to seal the structure.

Upon achieving sufficient strength in the strengthening layer grout, second-phase loading is initiated until complete failure of specimen occurs.



(a) first casting (b) second casting (c) covering plate

Fig. 5 Casting grout.

2.3 Loading and measurement

The testing was conducted in the *Structural Laboratory at Chongqing Jiaotong University*. A four-column servo press machine with a capacity of 10,000 kN was employed to act vertical force to the specimens (see **Fig. 6**). To minimize strain lag effects, low-rate loading was applied, with the entire test conducted at a constant displacement rate of 0.02 mm/min, ensuring that the dynamic increase factor (DIF) approached 1.0 as closely as possible. Loading was discontinued once the applied load decreased and reached 85% of the ultimate capacity.

The reaction force of the specimens was measured using force sensors located on the loading plate beneath the press machine. Axial displacement was monitored using linear variable differential transformers (LVDTs), with data recorded by a static testing system, as shown in **Fig. 6**. Due to the significant variations in strain at the peaks, troughs, and flat segment of the corrugated steel plates, six strain measurement points were installed at these locations on both sides of the column at mid-height of the strengthened column specimens. Considering that the principal stresses are oriented orthogonally, strain gauges for each measurement point were affixed along both the transverse and longitudinal

directions of the corrugation pattern.

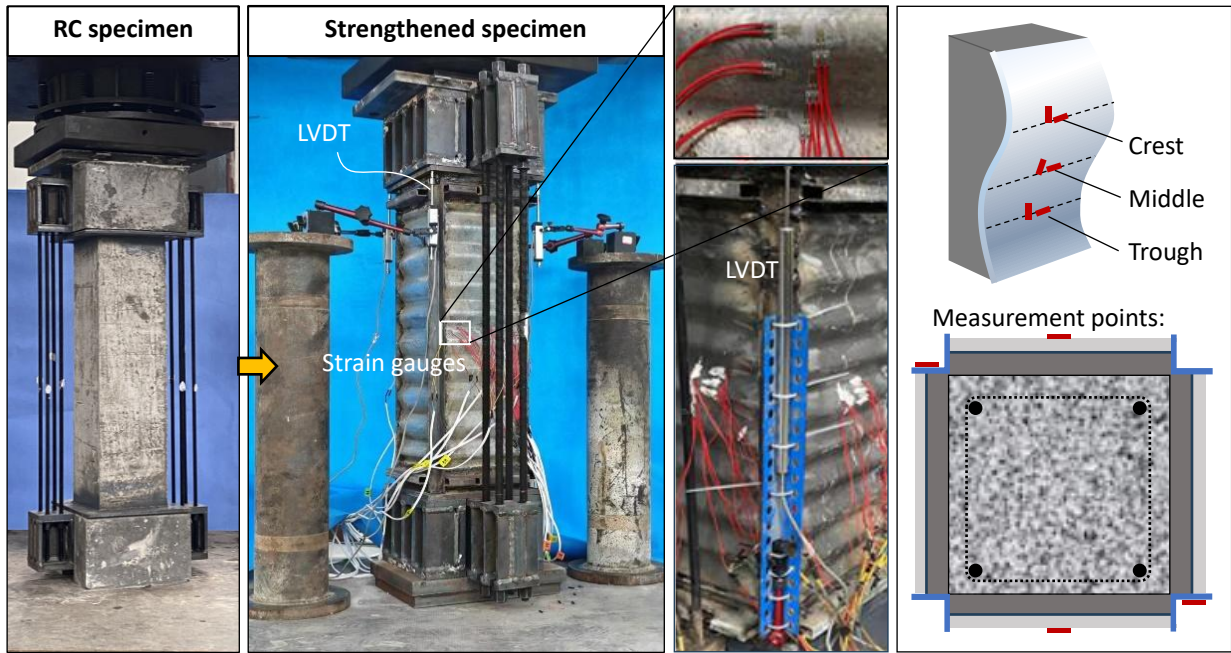


Fig. 6 Loading and measurement sets.

2.4 Material strength

2.4.1 Steel

To test the mechanical properties of steel, samples of corrugated steel plates, angle steels, and reinforcing bars were taken according to the provisions of *Metal Materials Tensile Test – Part 1: Method for Room Temperature Tests* (GB/T 228.1-2010) [46], *Steel for Reinforced Concrete – Part 2: Hot-Finished Ribbed Bars* (GB/T 1499.2-2018) [47], and the standard test methods and definitions for steel mechanical properties (ASTM A370-17a [48]). As shown in Fig. 7, due to the varying degrees of cold bending at different local positions on the corrugated steel plates, samples were taken from locations including peaks and flat segment of corrugated steel plates with different thicknesses. During tensile testing, loading was applied at a strain rate of 2.5×10^{-4} /s.



Fig. 7. Corrugated steel test

In practical engineering applications, the yield strength of corrugated steel plates is generally directly taken as the strength of the plate parent material. However, the increase in steel strength due to cold bending is considered as a safety margin. To accurately obtain the stresses in the experiment, the actual strength should be imported into the stress analysis model, this study adopted the yield strength after cold bending of the corrugated steel plate. The stress-strain tensile curve of cold-bent corrugated steel plates does not show an obvious yield plateau. Therefore, the yield strength was determined using the 0.2% residual strain method. The results are summarized in **Table 2**:

Table 2. Steel strength.

Tensile coupons	f_y /N/mm ²	f_u /N/mm ²
Corrugated segment ($t=1.6\text{mm}$)	332.81	356.97
Flat segment ($t=1.6\text{mm}$)	281.34	375.36
Corrugated segment ($t=2.0\text{mm}$)	389.42	437.31
Flat segment ($t=2.0\text{mm}$)	382.35	438.60
Corrugated segment ($t=2.7\text{mm}$)	413.99	464.85
Flat segment ($t=2.7\text{mm}$)	401.71	477.30
Angle steel ($t=4.0\text{mm}$)	346.56	523.27
Longitudinal bars ($d=12.0\text{mm}$)	443.20	589.46
Stirrups ($d=6.0\text{mm}$)	355.20	422.68

2.4.2 Concrete

The test used artificially configured concrete, with the 42.5 ordinary Portland cement. The mass ratio per cubic meter of concrete was as follows: cement/sand/aggregates/water = 376/704/1148/184. The water reducer dosage was 1.2% of the weight of the cementitious materials. During concrete pouring, nine 150-mm concrete cubes were arranged. These test cubes and specimens were all cured under the standard conditions as the specimens for 28 days, with an actual loading age of five months. In accordance with the *Code for Test Methods of Physical and Mechanical Properties of Concrete* (GB/T50081-2019) [49], the compressive strength tests were conducted using a 200-ton hydraulic testing machine at the Structural Testing Laboratory of the College of Civil Engineering, Chongqing Jiaotong University. The measured strength data deviating by more than 15% from the average strength value were excluded. As a result, the 28-days cubic compressive strength is 38.5 N/mm². In the time period of loading specimens, the average compressive strength of concrete cubes is 72.2 and 58.5 N/mm² corresponding to 2 different batches of concrete in specimens. The average compressive strength of prisms [49] is calculated as 54.9 and 44.5 N/mm², respectively.

2.4.3 Grout

According to the *Technical Specifications for Application of Cement-Based Grout Materials* (GB50488-2015) [50], when the maximum aggregate size in cement-based grout materials does not exceed 4.75 mm, the prism with dimensions of 40 mm×40 mm×160 mm is recommended to test the compressive strength. Considering the thin reinforcement layer thickness (t_g is 14-22 mm), six prisms with dimensions of 40 mm × 40 mm × 160 mm was used. The compressive strength test was conducted in accordance with the *Cement Mortar Strength Testing Method (ISO Method)* (GB/T 17671-2021) [51]. The average compressive strength of the grout prism was 37.1 N/mm².

3 Experiment Results

3.1 Failure modes

All specimens showed no significant damage until the applied load reached its peak. Only when the load began to decrease, minor buckling occurred at the corner steel angles, while the specimens remained intact overall, with no obvious lateral bulging (Figs. 8 and 9). It indicates that even with a steel plate thickness as thin as 1.6 – 2.7 mm, i.e., width-to-thickness ratios ranging from 74 to 125, sufficient confinement can still be achieved. It can be validated by comparisons of the load-displacement curves obtained from experimental tests and stress analysis results.

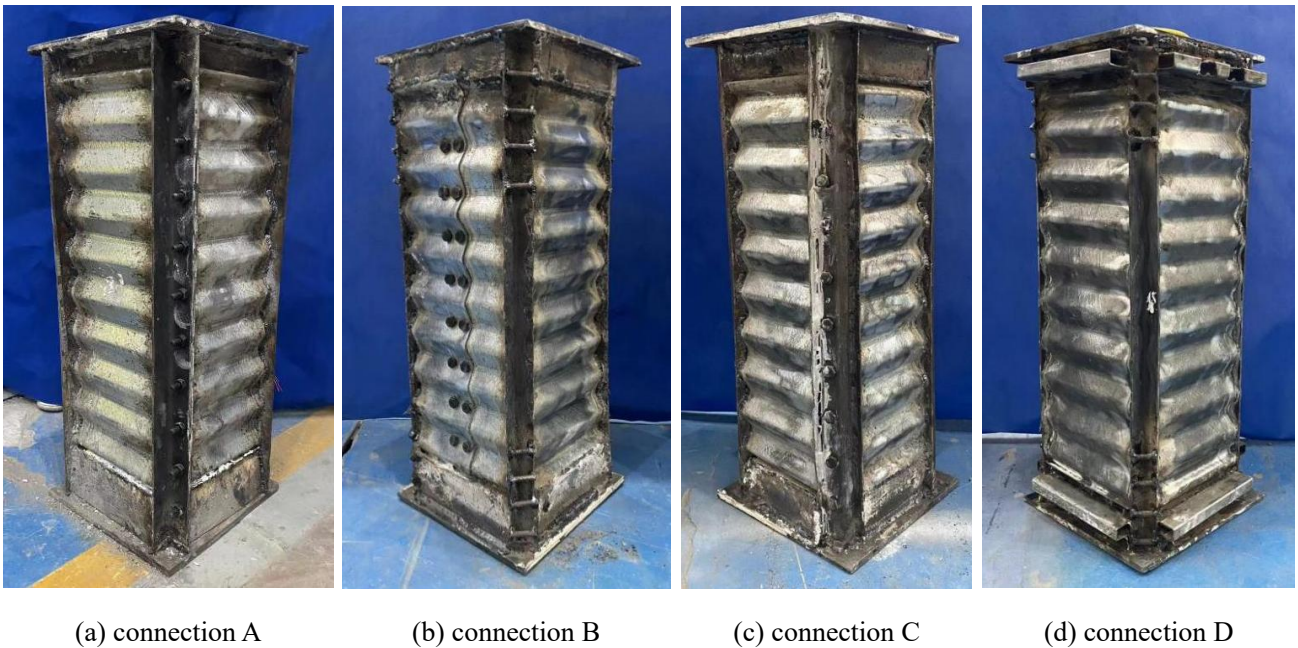


Fig. 8. Typical failure of specimens.

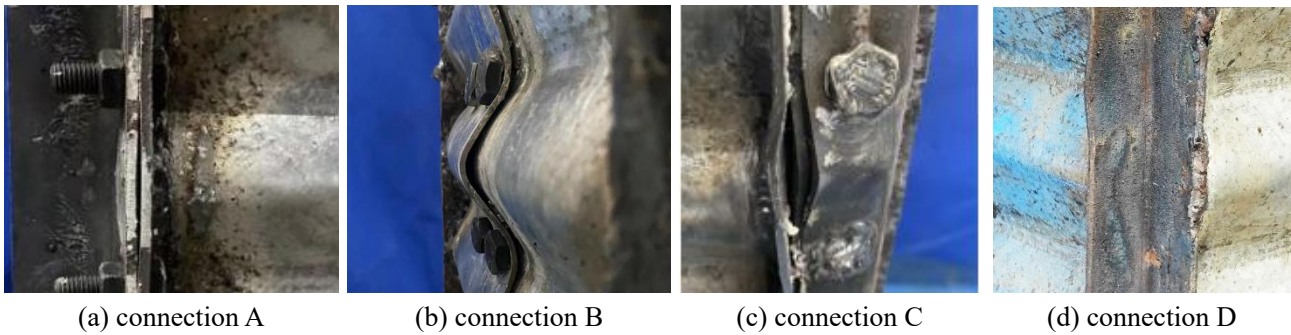


Fig. 9. Local failure in specimens.

For the specimen with Connection A, no significant damage occurred throughout the entire loading process. At 75% of the ultimate load, slight local buckling and loosening were observed between the two bolts at the mid-section's steel angles and flange plates.

For the specimen with the Connection B (Fig. 8), during the initial loading to peak load, no significant changes occurred on the external surface of the steel plates, angles, and the central connection of the corrugated steel sheets. As displacement increased further and loading was applied until the load reached 80% of the ultimate load (i.e., 2500 kN), minor buckling occurred at the corner angles. When the load was reduced to 60% of the ultimate load (1900 kN), a peeling trend was observed between the two corrugated steel sheets at the central connection, with slight lateral bulging of the adjacent steel plates.

For the specimen with Connection C, no significant changes occurred until the load was reduced to 90% of the ultimate load. At that moment, a muffled sound was heard, suggesting potential crushing of the core concrete or grout between the layers. Continued loading to 50% of the ultimate load resulted in local buckling and separation of the two corner connected parts, while the bolts remained intact without loosening.

For the specimen with Connection D, including specimens with different damage levels (different initial axial compression ratios), no significant phenomena can be observed until the load was reduced to 70% of the ultimate load.

3.2 Load-Displacement Curves

During the early stages of loading, even though the core concrete had developed some plastic behavior, the rest of the concrete remained in the elastic working stage due to the enhanced section. As a result, the curve initially exhibited roughly linear-elastic behavior. When the load increased and exceeded the original ultimate bearing capacity of the RC section, the specimen curve began to show

curvature, with the onset of plastic deformation. Upon reaching the critical state, the load started to decrease, and the peak deformation corresponding to the load was approximately twice the original RC section's peak deformation. The ductility in the descending segment was also significantly better than that of the plain RC specimens.

From the comparison, it can be observed that after being wrapped with sleeves and having its section enlarged, the ultimate bearing capacity was significantly strengthened. Although some cracking occurred under the initial axial compression, potentially reducing the strength, the constrained concrete's strength was enhanced due to the confinement effect. As a result, the ultimate bearing capacity increased from 2117.7 kN to 2850.9 - 3543.4 kN, representing an increase of 34.6% to 67.3%.

As compared in **Fig. 10**, there is no obvious impact on the load-to-displacement curves of specimens with different thickness of the corrugated steel jacket. It suggests that the confinement of the corrugated steel jacket may not be taken full advantage. As well, the enhanced ultimate capacity and ductility are both far greater than that of the original RC section, indicating that it may be unnecessary to design a thick jacket.

The comparison in **Fig. 11** shows little difference among the four connection types in terms of ultimate bearing capacity. However, regarding connection strength, the specimen Connection D with full welding at the corner has the highest strength, resulting in the most reliable radial confinement. As shown in **Table 1**, the concrete compressive strength of CS-D-1.6-0.4 is 54.9 N/mm², 23.4% higher than the other 3 specimens with different connection (44.5 N/mm²). As a result, its ultimate bearing capacity (3361.3 kN) is 9.8% greater than the mean value other 3 specimens. In specimen Connection C, a sharp drop in load occurred when residual load was reduced to 3000 kN, potentially due to the steel plate at the corner experiencing reduced effective cross-section and decreased compressive stiffness because of openings or dense welds, leading to local buckling. However, after reaching around 2000 kN, the load decline slowed down as residual capacity was regained due to circumferential confinement. For specimen Connection B, its bearing capacity is moderate. After loading ended, only slight gaps were observed at the wave plate connections. Compared to other connection forms, this might represent the most suitable connection type. The specimen Connection A exhibits unique behaviour: its load bearing capacity remained stable for a period after reaching peak load. However, when compressive displacement reached 4 mm (compression strain = 0.005), local instability failure

occurred due to multi-wave buckling of the angle steel, causing a sudden drop in bearing capacity. As lateral confinement became effective, the rate of load decline slowed down.

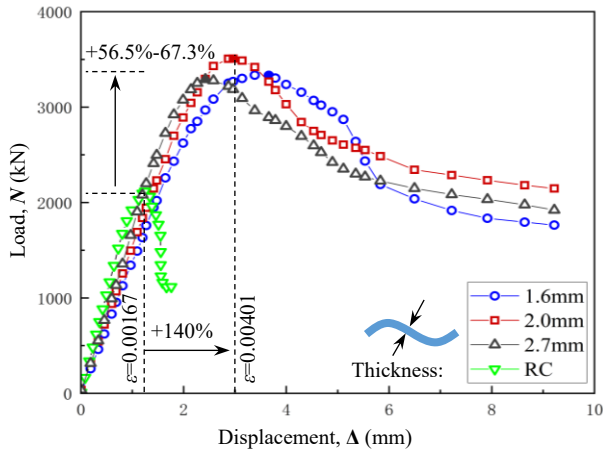


Fig. 10. Influence of thickness of jacket.

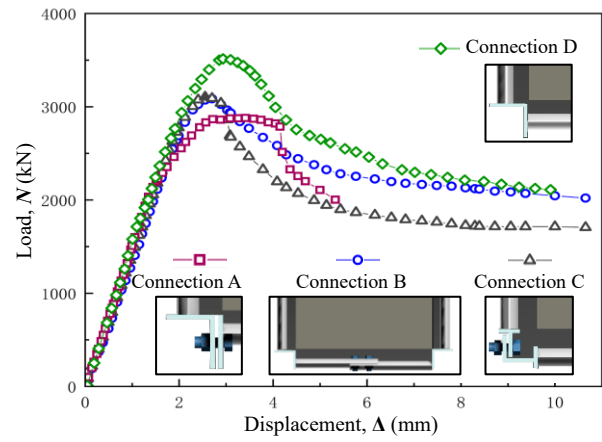


Fig. 11. Influence of connection type.

As shown in **Fig. 12**, the performance enhancement of RC sections strengthened at different initial damage rates varies in the load-displacement ($N-\Delta$) curves. The load bearing capacity of the strengthened specimens decrease with the increasing initial compression ratio. For initial axial compression ratios of 0.4 and 0.6, the $N-\Delta$ curves are relatively similar; nevertheless, an increase in the initial axial compression ratio still results in reduced reinforcement improvement effects. For the specimens with an initial axial compression ratio from 0.4 to 0.6, the increase in bearing capacity compared to the RC section decreases from 67.3% to 60.0%. However, in extreme cases where the initial axial compression ratio reaches 1.0 (i.e., concrete stress reaches the ultimate strength value), the concrete softens remarkably, with its modulus and residual strength sharply decreasing. Therefore, enhancing confinement of the section results in a significant reduction in initial stiffness. Yet, the ultimate bearing capacity still increases by 34.6% compared to the original RC section. The softening is not only reflected in load-bearing capacity but also in deformation capacity. Based on the increased confinement factor due to reduced concrete strength, it can be deduced that more severe damage to the reinforced section may lead to greater peak deformation, as the outer jacket provides relatively stronger confinement.

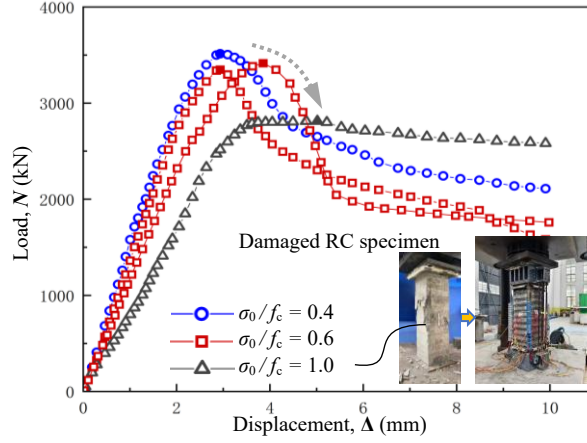


Fig. 12. Influence of initial damage.

3.3 Strength index and ductility index

As the concrete strength was not completely the same in the test, a further analysis is necessary based on dimensionless indicators. The strength index (SI) [52] can be used for estimate the load carry capacity of an ordinary reinforced concrete section strengthened by corrugated steel jacket, which can be calculated as following:

$$SI = \frac{N_u}{f'_c A_c + f_{c,g} A_g + f_s A_s} \quad (1)$$

where N_u , f_s and A_s are respectively the ultimate load bearing capacity of the column, compressive strength and sectional area of longitudinal bars.

The ductility index, DI , well represents the deformation capacity and energy absorption of a structural member [52]. As shown below:

$$DI = \varepsilon_{85\%} / \varepsilon_y \quad (2)$$

where $\varepsilon_{85\%}$ and ε_y are the axial compressive strain corresponding to $0.85N_u$ in the descending stage and yield compressive strain. The ε_y can be obtained using the farthest point method proposed by Feng P et. al. (2017) [53].

The confinement factor, ζ , is an important index to assess the mechanical behaviour of concrete-filled tubular columns [52]. If the columns were not damaged, the ζ should be slightly minor. Because the confining tube is constructed after the damaged of concrete, the residual compressive strength of the concrete with damage (f'_c) should be employed to calculate ζ :

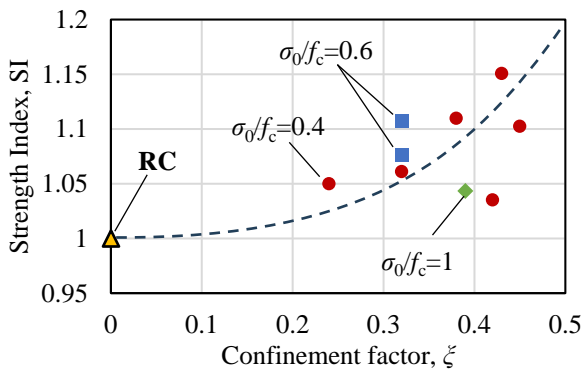
$$\zeta = \frac{f_{y,cs} A_{cs} + f_{y,L} A_L}{f'_c A_c + f_{c,g} A_g} \quad (3)$$

where f'_c , $f_{c,g}$, $f_{y,cs}$, $f_{y,L}$ and A_c , A_g , A_{cs} , A_L are respectively the compressive strength of damaged concrete and grout, yield strength of corrugated steel sheet and angle steel, and the areas of them.

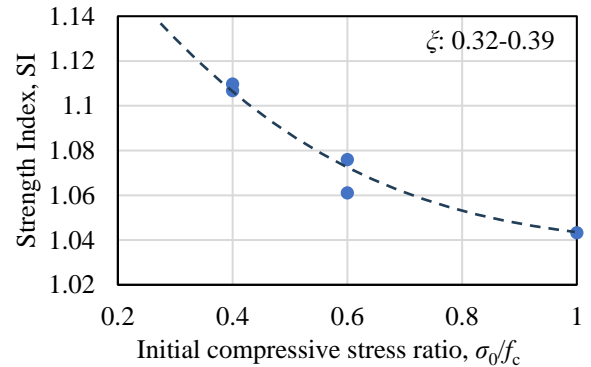
As shown in **Fig. 13**, the strength index (SI) and ductility index (DI) exhibit a strong dependence on two key parameters: the confinement factor (ξ) and the initial compressive stress ratio (σ_0/f_c). Increased ξ enhances both SI and DI , reflecting enhanced confinement effects. In contrast, the initial compressive stress ratio (σ_0/f_c) influences SI and DI differently. The increase in σ_0/f_c reduces SI due to more cracks developing in the concrete, while it simultaneously enhances DI due to the softening behavior of the concrete. In terms of the connection type of corrugated steel jacketing, CS-B-2-0.4 shows a similar DI to CS-D-2-0.4, indicating that the bolts connection may have a satisfactory strength as the welding in the corner if the design of connection strength is rational.

Table 3. SI and DI of specimens

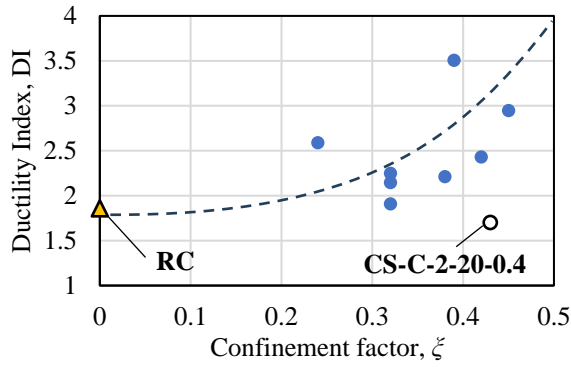
No.	Specimens	σ_0 (MPa)	α	ξ	N_0 (kN)	N_u (kN)	SI	DI
1	RC	0	0	0	/	2117.7	1.0	1.86
2	CS-A-2-0.4	$0.4f_c$	5.45%	0.45	2733.5	2957.4	1.082	2.95
3	CS-B-2-0.4	$0.4f_c$	4.25%	0.38	2845.2	3101.1	1.090	2.21
4	CS-C-2-0.4	$0.4f_c$	4.88%	0.43	2767.1	3125.6	1.130	1.70
5	CS-D-1.6-0.4	$0.4f_c$	3.64%	0.24	3264.2	3361.3	1.030	2.59
6	CS-D-2.7-0.4	$0.4f_c$	5.23%	0.42	3264.2	3314.0	1.015	2.43
7	CS-D-2-0.4	$0.4f_c$	4.22%	0.32	3264.2	3543.4	1.086	2.25
8	CS-D-2-0.6a	$0.6f_c$	4.22%	0.32	3249.4	3365.8	1.036	1.91
9	CS-D-2-0.6b	$0.6f_c$	4.22%	0.32	3249.4	3412.9	1.050	2.14
10	CS-D-2-1.0	$1.0f_c$	4.22%	0.39	2821.7	2850.9	1.010	3.51



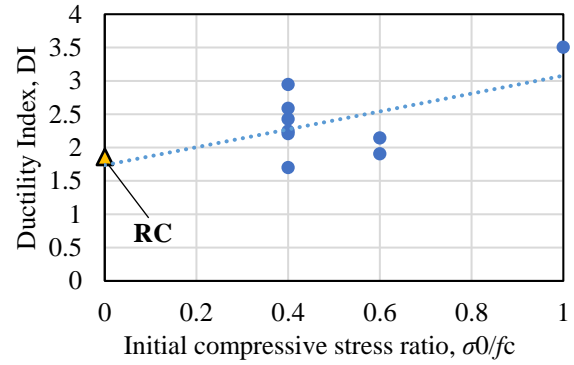
(a) impact of confinement factor on SI



(b) impact of initial compressive stress on SI



(c) impact of confinement factor on DI



(d) impact of initial compressive stress on DI

Fig. 13 Influence factors on SI and DI .

4 Confinement Mechanism

4.1 Load Carrying Mode

Previous studies on corrugated steel concrete columns have shown that the primary role of the corrugated steel is to provide circumferential confinement [35][36][38]. Similarly, in reinforced concrete sections strengthened with corrugated steel plates, the outer corrugated steel plates bear minimal longitudinal loads and mainly provide lateral confinement. The parts directly carry the axial load include the original RC section, the reinforcement layer grout, and the corner connection components of the sleeves. It can be verified by examining the development patterns of strain and stress.

4.1.1 Strain of corrugated jacket

The strain of corrugated steel plates is influenced by their corrugation profile, with variations in strain occurring across the crests, troughs, and flat segment within one period of corrugation. For transverse strain, overall tensile strain is relatively small, possibly due to the placement of strain gauges farther from the corners, where the confinement is the greatest in a square or rectangular cross section [54]-[57]. In the middle regions, steel does not need to provide significant confinement, resulting in reduced transverse tensile strain. For longitudinal strain, the trough of the corrugated steel plate exhibits a more pronounced compressive longitudinal strain, indicating that the concave trough may take on part of the load. Conversely, the crest shows nearly zero longitudinal strain, suggesting that the convex crest relieves some of the applied stress. This phenomenon, known as the “bending effect,” was proposed by Wang and Yang et al. (2019) [36] under compressive loading conditions.

4.1.2 Stresses of corrugated jacket

To observe the load bearing mode of the corrugated jacket, the stresses of CSP is calculated by using the elastic-plastic analysis [35][36][58]. Based on the transverse and longitudinal strain, the stress components and Mises stress at the crest, middle and trough on the outer surface of corrugated plates are obtained.

(1) Plane elastic-plastic analysis method

For the stress at different positions on the corrugation, the respective Poisson's ratio, elastic modulus, and steel yield strength are incorporated into the calculations to obtain a more precise analysis of the corrugated steel plate stress. Since the corrugations in the steel plates run horizontally, the principal stresses in the columns under axial compression are primarily in the horizontal and vertical directions. Given that the shear stress within the corrugated steel plates is relatively small, only these two directional normal stresses were analyzed in the test.

In the elastic stage, the stress components meet the generalized Hooke's Law:

$$\begin{bmatrix} \sigma_h \\ \sigma_v \end{bmatrix} = \frac{E_s}{1 - \mu_s^2} \begin{bmatrix} 1 & \mu_s \\ \mu_s & 1 \end{bmatrix} \begin{bmatrix} \varepsilon_h \\ \varepsilon_v \end{bmatrix} \quad (4)$$

where ε_h , ε_v , σ_h , σ_v , E_s and μ_s are respectively the horizontal strain, vertical strain, horizontal stress, vertical stress, elastic modular and Poisson ratio.

In the elastic-plastic stage, the E_s and μ_s can be replaced by the tangential modular (E_s^t) and elastic-plastic Poisson ratio (μ_{sp}):

$$\begin{bmatrix} \sigma_h \\ \sigma_v \end{bmatrix} = \frac{E_s^t}{1 - \mu_{sp}^2} \begin{bmatrix} 1 & \mu_{sp} \\ \mu_{sp} & 1 \end{bmatrix} \begin{bmatrix} \varepsilon_h \\ \varepsilon_v \end{bmatrix} \quad (5)$$

$$E_s^t = \frac{(f_y - \sigma) \sigma}{(f_y - f_p) f_p} E_s \quad (6)$$

$$\mu_{sp} = 0.283 + 0.167 \frac{\sigma - f_p}{f_y - f_p} \quad (7)$$

The stress-strain relation is more complex in the plastic stage, which can be expressed by:

$$\begin{bmatrix} \sigma_h \\ \sigma_v \end{bmatrix} = \frac{E_s}{Q} \begin{bmatrix} \sigma_v'^2 + 2p & 2\mu_s p - \sigma_h' \sigma_v' \\ 2\mu_s p - \sigma_h' \sigma_v' & \sigma_v'^2 + 2p \end{bmatrix} \begin{bmatrix} \varepsilon_h \\ \varepsilon_v \end{bmatrix} \quad (8)$$

where the parameters can be calculated by the following equations (9-14).

$$\sigma_h' = \sigma_h - \sigma_{cp} \quad (9)$$

$$\sigma'_v = \sigma_v - \sigma_{cp} \quad (10)$$

$$\sigma_{cp} = \frac{\sigma_h + \sigma_v}{3} \quad (11)$$

$$H' = \frac{d\sigma}{d\varepsilon_p} = 3 \times 10^{-3} E_s \quad (12)$$

$$Q = \sigma_h'^2 + \sigma_v'^2 + 2\mu_s \sigma_h' \sigma_v' + \frac{2H'(1-\mu_s)\sigma_z^2}{9G} \quad (13)$$

$$\sigma_z = \sqrt{\sigma_h^2 + \sigma_v^2 - \sigma_h \sigma_v} \quad (14)$$

(2) Strain and stress analysis result

Since strain was recorded on both sides of the cross-section at the same position in the corrugation, two load-strain curves were obtained, as shown in **Figs. A-1** and **A-2**.

The horizontal strain or stress of the corrugated steel jacket represents the degree of confinement. During the ascending stage of loading, it exhibits a slight tensile increase. In the descending stage, the horizontal strain generally decreases rapidly at both the crest and trough of the corrugation, or even become compressive. Only the middle of corrugation remains tensile. This behavior may be attributed to the Poisson effect, where increasing vertical compressive strain suppresses horizontal tensile strain. For the specimen CS-D-2-1.0 with complete damage, the horizontal strain at one of the measured points has approached the yield strain, and horizontal stress can reach near 200N/mm² at the ultimate load. It indicates that the initially damaged concrete has a more significant lateral expansion, which is prevented by the corrugated steel sheet. However, the horizontal strain and stress become minor with less damage, suggesting that the cracking and softening of the damaged concrete can increase the confinement effect in the round strengthened RC column. The corrugated steel sheet should have exhibited good confinement [35], whereas, it was not taken full advantage due to the reduced confinement development in a square section[79].

For vertical strain and stress, similar behavior can be observed in concrete-filled corrugated steel tubes with circular cross-sections [35]. During compression of the corrugated steel together with the column, the outer-surface fibers are stretched at the peak and flat segments of the corrugation, where tensile and compressive stresses cancel each other. Conversely, the trough is compressed more with the superimposing of column compressive stress, resulting in greater compressive stress. This

superposed stress causes the Mises stress at the trough to increase significantly faster than at the crest and flat regions of the corrugation (**Fig. A-2**). As shown in **Fig. 13 (b)**, the average longitudinal stress of all specimens in the corrugated steel was only -3.591 MPa by using weighted mean values[35], indicating that the axial load directly borne by the corrugated steel plate can be negligible. This finding is consistent with previous relevant research conclusions[36][38][39][57].

In general, the corrugated steel plates at different positions exhibit low stress levels, with most horizontal stresses and vertical stresses not exceeding 100 N/mm², and the Mises stress not reaching the yield strength value (**Fig. 13(c)**). The exception occurs when severe plastic strain develops in the initial RC section with complete damage. Given this low stress level, the thickness of the corrugated steel does not need to be excessively large; it only needs to satisfy the construction requirements for local stability and connection reliability.

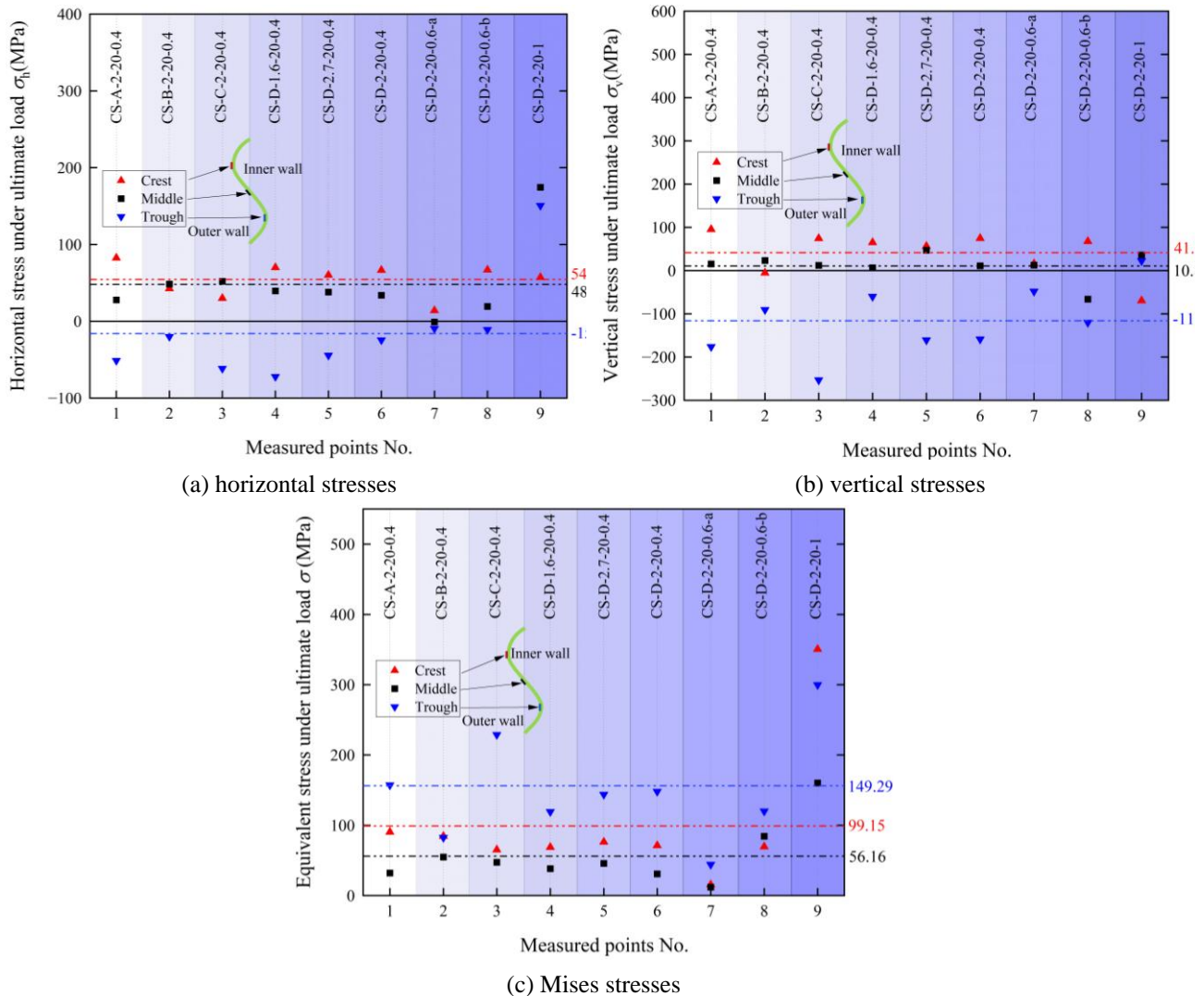


Fig. 13. Stress components and Mises stress at ultimate load.

5 Ultimate axial load bearing capacity

5.1 Ultimate state mechanics

To facilitate the calculation and design of the ultimate bearing capacity of reinforced concrete sections after strengthening, the stress distribution across the section at the ultimate load-bearing state is analyzed as shown in **Fig. 14**. The reinforced concrete sections after strengthening are no longer ordinary but have become a composite section confined by the jacket, with its load-bearing mechanism similar to that of square steel tube concrete columns [57]. In the regions close to the corners, the confinement is strong, whereas, it becomes weaker near the centerlines on the sides. Therefore, when the column is under compression, the concrete and grout in regions A1 and A3 (confined areas) are subjected to triaxial compression. Conversely, in the areas A2 and A4 that is weakly confined or unconfined, the concrete may even experience uniaxial compression. To accurately calculate the ultimate bearing capacity of such sections, it is necessary to analyze each region separately and then combine the results. In the calculations, the boundary between the strongly confined and weakly confined zones is assumed to be a quarter-circle arc. Based on this assumption, the areas of each partition can be computed as detailed.

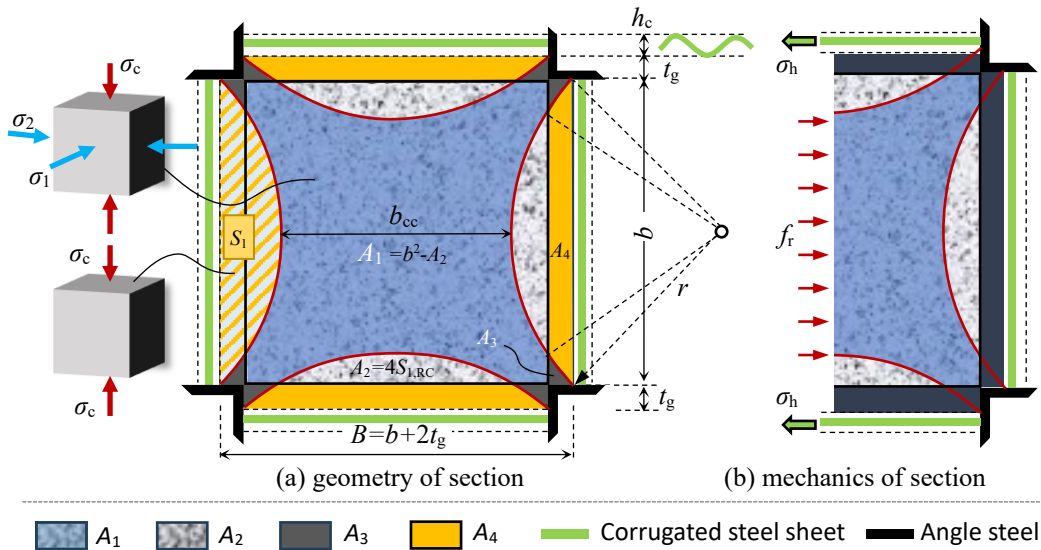


Fig. 14. Force analysis of cross section.

$$r = \frac{\sqrt{2}}{2} b \quad (15)$$

where the B , b , r , h_c are width of enhanced RC section, width of grout layer, imaginary radius of unconfined zone, and corrugation depth.

(1) Section geometry

With the r , the single unconfined zone area and the unconfined RC section area can be easily calculated by **Eqs. (16)** and **(17)**.

$$S_1 = \frac{(\pi-2)r^2}{4} \quad (16)$$

$$S_{1,RC} = r^2 \arccos\left(\frac{\sqrt{2}}{2} + \frac{t_g}{r}\right) - (\sqrt{2}r + 2t_g)\sqrt{\frac{r^2}{2} - \sqrt{2}t_g r - t_g^2} \quad (17)$$

As the partition shown in Fig. 16, the corresponding area can be calculated by using **Eqs. (18) – (21)**, where the edges between unconfined and confined area is assumed to be arc lines.

$$A_1 = b^2 - A_2 \quad (18)$$

$$A_2 = 4S_{1,RC} \quad (19)$$

$$A_3 = B^2 - [A_1 + A_2 + A_4 + 4(L_s - t_0 - h_s)^2] \quad (20)$$

$$A_4 = S_1 - S_{1,RC} \quad (21)$$

(2) Strength models

For the A1 region, the concrete core is confined in a damaged state and thus its compressive strength should account for corresponding plastic damage. In this confined region, the confined concrete compressive strength should be taken into analysis of load bearing capacity.

There are plenty of strength model for confined concrete, which is primary related to the confining stress.

Table 4 Strength models for confined concrete

Type I: $f_{cc}/f_{co} = a + k(f_r/f_{co})^b$		
Park R. et al. [59]	square confined concrete	$f_{cc} = f_{co} + 2f_r$
Hoang L. et al.[60]	circular steel tube confined concrete	$f_{cc} = f_{co} + 3.16f_r$
Richart E.[61]	combined compressed concrete	$f_{cc} = f_{co} + 4.1f_r$
Eurocode 2 [62]	concrete filled steel tube	$f_{cc} = f_{co} + 5f_r, f_r < 0.05f_{co}$
Zhou X. et al. [63]	square confined concrete	$f_{cc} = f_{co} + 5.1f_r$
Candappa D. et al.[64] and Wang Y. et al.[36]	concrete under triaxial compression	$f_{cc} = f_{co} + 5.3f_{co}$
Saatcioglu M. et al.[65]	confined concrete	$f_{cc} = f_{co} + 6.7f_r^{0.83}$
Hoshikuma J. et al.[66]	confined concrete	$f_{cc} = f_{co} + 7.6f_r$

Fafitis A. et al.[67]	confined concrete	$f_{cc} = f_{co} + \left(1.15 + \frac{21}{f_{co}}\right) f_r$
Type II: $f_{cc} = k f_{co}$		
Mander J. et al.[68]	stirrups confined concrete	$f_{cc} = f_{co} \left(-1.254 + 2.254 \sqrt{1 + 7.94 \frac{f_r}{f_{co}}} - 2 \frac{f_r}{f_{co}} \right)$
Attard M. [69]	confined concrete	$f_{cc} = f_{co} \left(\frac{f_r}{f_t} + 1 \right)^{1.25 f_c^{-0.21} (1 + 0.062 f_r / f_{co})}$
Setunge S. et al.[70]	confined high-strength concrete	$f_{cc} = f_{co} (1 + 13.07 f_r / f_{co})^{0.63}$
Cusson D. et al.[71]	confined high-strength concrete	$f_{cc} = f_{co} \left[1 + 2.1 (f_r / f_{co})^{0.7} \right]$
Legeron F. et al.[72]	confined normal & high-strength concrete	$f_{cc} = f_{co} \left[1 + 2.4 (f_r / f_{co})^{0.7} \right]$
Bousalem B. et al.[73]	rectangular confined concrete	$f_{cc} = f_{co} \left(1 + 0.8 \frac{f_r}{\sqrt{f_{co}}} \right)$
Girgin Z. et al. [74]	confined ultra-high-strength concrete	$f_{cc} = f_{co} \left[1 + 4.08 \left(\frac{f_r}{f_{co}} \right)^{0.83} \right]$

Note: the f_{cc} , f_{co} and f_r are the confined concrete compressive strength, compressive strength of plain concrete and confining stress, respectively.

The listed models provide two typical calculation modes for the concrete under triaxial compression, including linear and non-linear equations. However, the models are proposed based on different test conditions, which may lead to discreteness in predicting the strength of concrete confined by square corrugated steel jacket.

Megahed K., et al. (2024) [75] have validated the strength model proposed by Lim. J. and Ozbakkaloglu T. (2014) [76] based on 1041 previously tested CFST stub columns, including 337 rectangular short column specimens. As recommended in **Eq. (22)**, the confined concrete strength, f'_{cc} , is determined by the confining stress (f_r).

$$f'_{cc} = f'_c + 5.2 f'_c{}^{0.91} \left(\frac{f_r}{f'_c} \right)^{f'_c - 0.06} \quad (22)$$

where f'_c is the compressive strength of concrete with damage.

As shown in **Fig. 14**, the f_r can be obtained by the equilibrium equation between the resultant forces of corrugated steel tube and confined concrete in A1 section:

$$f_r = \frac{\eta_{cs} t_{cs} \sigma_h}{B - (2 - \sqrt{2})b} \quad (23)$$

where t_{cs} , η_{cs} and ε_0 are respectively the concrete compressive strength of original RC column, and compressive strain at the peak, and the compressive concrete strain under permeant load.

For the A2 region, the compressive strength of concrete with damage (f'_c) should be employed, and the influence of damage can be expressed as **Eq. (24)**.

$$f'_c = f_c \left(1 - k_d \sqrt{\frac{\varepsilon_0}{\varepsilon_c}} \right) \quad (24)$$

where the compressive strain in the concrete at the peak stress $\varepsilon_c = 0.7f_c^{0.31}$ (EC2 [62]). For the strengthened concrete column suffering damage, the f'_c should be employed to calculate the ultimate load bearing capacity. A strength loss factor (k_d) can be then utilized to characterize the reduced strength caused by the damage. As per the study on concrete-filled corrugated steel tube under cyclic axial compression (Fang & Wang et. al. 2021&2023)[77][78], k_d can be obtained between 0.04 to 0.10 at the ultimate state. In this analysis, 0.1 is used to conservatively estimate the strength considering damage. To better describe the rule of the loss of strength in different damage stages, the initial damage ratio $\varepsilon_0/\varepsilon_c$ is proposed herein, to further match the f'_c with the corresponding damage.

Similarly, for the A3 zone, the infilled grout is confined without damaged before loading. Therefore, the confined compressive strength of grout ($f_{cc,g}$) should be adopted to calculate the load bearing capacity, which is given by **Eq. (25)**. For the A4 zone under less confinement, the compressive strength of grout ($f_{c,g}$) is directly employed to calculate the capacity.

$$f_{cc,g} = f_{c,g} + 5.2 f_{c,g}^{0.91} \left(\frac{f_r}{f_{c,g}} \right)^{f_{c,g}^{-0.06}} \quad (25)$$

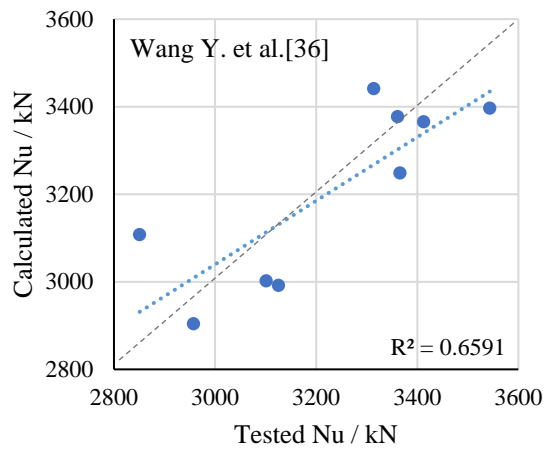
where $f_{cc,g}$ and $f_{c,g}$ are confined reinforcement material compressive strength, and reinforcement material compressive strength, respectively.

The corrugated steel jacketed square RC column can be regarded as a type of confined concrete column [79]. As proven above, the corrugated steel sheet, especially near the centerline of cross section, does not directly bear axial load. Therefore, only the corner angle steels, reinforcing layer grout, core concrete, and reinforcement bars are considered to carry the load. The axial compressive load-bearing capacity of the strengthened RC section (N_u) can be calculated by:

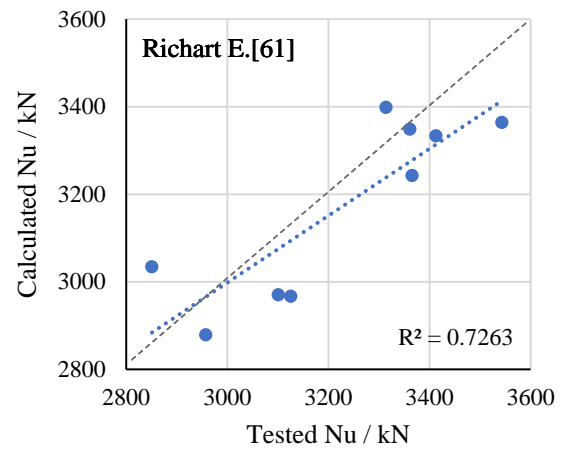
$$N_u = f'_{cc}A_1 + f'_c A_2 + f_{cc,g}A_3 + f_{c,g}A_4 + f_L A_L + f_{yb}A_b \quad (26)$$

where the f_L , f_{yb} , A_L , A_b are yield strength of angle steel and original longitudinal rebars, areas of angle steel and longitudinal rebars, respectively.

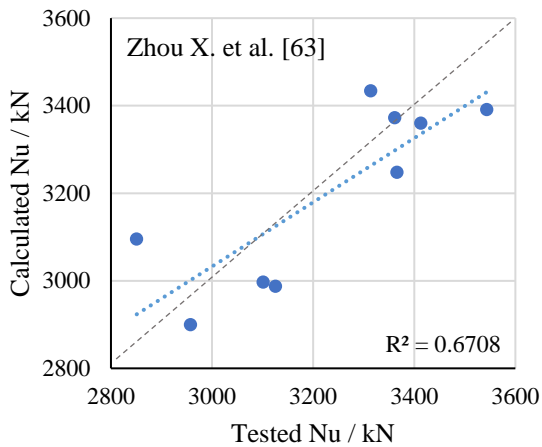
Due to the RC section encapsulated with corrugated sheets possessing characteristics of confined concrete, the confined concrete strength model is applicable to the RC column rehabilitated with corrugated jacketing. As compared in **Fig. 15**, substituting various confinement concrete strength models into **Eq. (26)** can accurately predict the ultimate bearing capacity, consistent with expectations.



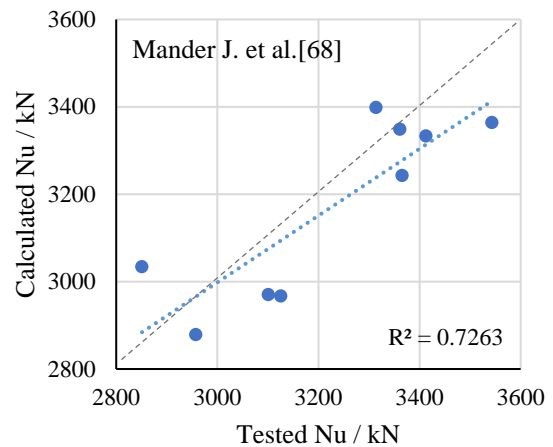
(a) concrete-filled corrugated steel tube model



(b) hydraulic pressure confined concrete model



(c) square CFST strength model



(d) spiral stirrups confined concrete model

Fig. 15. Different strength models for load bearing capacity, Nu.

As validated in **Fig. 16**, considering the contributions of each component to bearing capacity, the initial damage in the concrete core, and the enhancing effect of confinement on the concrete strength, the calculated bearing capacity using proposed **Eqs. (22)-(26)** closely matches the test piece actual measurements, with an average error of 1.86%. It provides an accurate calculation method for predicting the ultimate bearing capacity of the reinforced section.

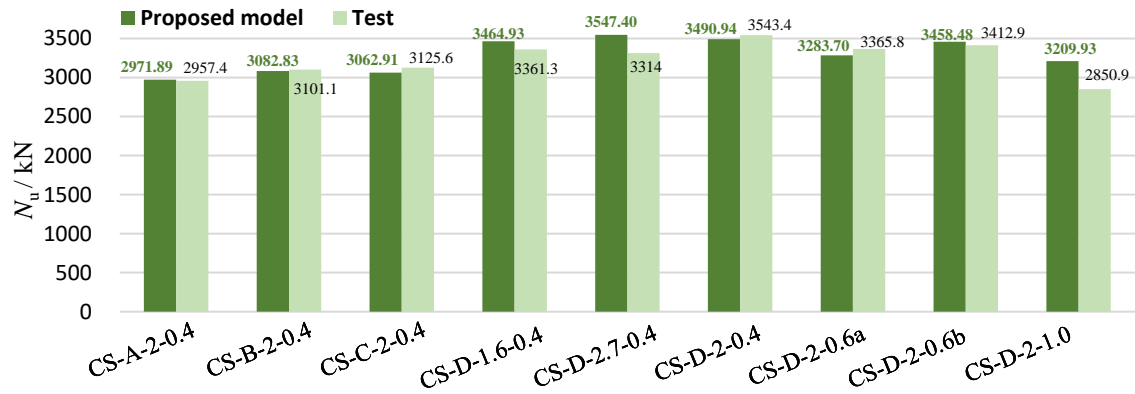


Fig. 16. Validation of proposed model for ultimate capacity.

6 Conclusions

In this study, the axial behavior of damaged RC short columns strengthened by using corrugated steel jackets is studied experimentally. Ten columns were tested to investigate the influence of the connection methods for corrugated sheets, corrugated steel thickness, and damage levels on load-displacement curves, as well as stress and strain development patterns. By comparing different strength model of confined concrete, a calculation method for the enhanced RC section is developed considering axial compression ratio and transverse confinement. The following conclusions can be drawn:

(1) From the experimental results of strengthening square reinforced concrete columns with corrugated steel sleeves, it is evident that the improvement effect is significant. Adding corrugated steel sleeves to damaged reinforced concrete columns can increase the ultimate bearing capacity of the original RC short columns from 2117.7 kN to 2850.9–3543.4 kN, with an increase of 34.6%–67.3%.

(2) Due to the insufficient confinement effect in square sleeves, the thickness of the corrugated steel sleeves has little noticeable impact on the load-displacement curves of the specimens. Furthermore, the significant improvement in ultimate bearing capacity and ductility after strengthening far exceeds the original reinforced concrete sections. This suggests that, when strengthening square columns, there may be no need to use corrugated steel sleeves with thicker walls, as long as the stability in construction is ensured.

(3) Under different connection types, the differences in ultimate bearing capacity and ductility are minimal. Therefore, in practical engineering applications, bolted connections can achieve results comparable to corner-welded connections, provided that rational connection design is achieved.

(4) More severe damage to the reinforced section may lead to better deformation capacity, as the loss of concrete strength results in an increased confinement factor. Observations reveal that the performance enhancement of RC sections strengthened at different initial damage rates varies in the load-displacement curves. For specimens with an initial axial compression ratio ranging from 0.4 to 1.0, the shortening displacement at the peak load increases from 3 mm to 5 mm. However, the damage causes the concrete to soften, resulting in a decrease in the load-bearing capacity of the strengthened specimens as the initial compression ratio increases.

(5) The lateral stress in the corrugated steel sheet determines the magnitude of the confinement stress in the concrete. While the corrugated steel sheet exhibits good confinement properties, its full potential is not utilized in square sections due to reduced confinement development. Only when the concrete core is severely damaged does the lateral strain and stress increase significantly. For the specimen CS-D-2-1.0 with complete damage, the lateral strain at one of the measurement points approaches the yield strain, and the lateral stress reaches nearly 200 N/mm² at ultimate load. This suggests that the cracking and softening of damaged concrete can enhance the confinement effect in corrugated steel-strengthened RC columns. The longitudinal stress in the corrugated steel sheet exhibits characteristics of bending effects, and the average longitudinal stress throughout the cycle remains at a relatively low level, indicating that the corrugated steel sheet does not directly bear significant loads.

(6) The strength index (*SI*) and ductility index (*DI*) exhibit a strong dependence on two key parameters: the confinement factor (ζ) and the initial compressive stress ratio (σ_0/f_c). Increased ζ enhances both *SI* and *DI*, reflecting enhanced confinement effects. In contrast, the σ_0/f_c influences *SI* and *DI* differently. An increase in σ_0/f_c reduces *SI* due to the development of more cracks in the concrete, while it simultaneously enhances *DI* due to the softening behavior of the concrete.

(7) The confined concrete strength model is applicable to RC columns strengthened with corrugated steel jackets. It can be used to accurately predict the ultimate bearing capacity, with only 1.86% deviation.

References

- [1] Michael A. L., Abhishek G., Travis M. Chapter 6 - Durability of buildings and building elements under a changing climate: A Canadian perspective[J]. *Living with Climate Change*, 2024. 101-124.
<https://doi.org/10.1016/B978-0-443-18515-1.00011-3>
- [2] Yang Q.S., Yin J.Q. et., al. Post-disaster investigations of damage feature of buildings and structures due to several local strong winds in China during 2021–2024[J]. *Advances in Wind Engineering*, 2024. 1(2):100011.
<https://doi.org/10.1016/j.awe.2024.100011>
- [3] Yang, D., Liu, F., Huang, SS. *et al.* Fire Behaviour of Rectangular Steel Tubed-Reinforced-Concrete Columns with End Restraints. *Int J Steel Struct* **24**, 1406–1421 (2024). <https://doi.org/10.1007/s13296-024-00898-5>
- [4] Luo, H.Y., Zhang, L.L. & Zhang, L.M. Progressive failure of buildings under landslide impact. *Landslides* **16**, 1327–1340 (2019). <https://doi.org/10.1007/s10346-019-01164-0>
- [5] Jin S., Du H., Bai J. Seismic performance assessment of steel frame structures equipped with buckling-restrained slotted steel plate shear walls[J]. *Journal of Constructional Steel Research*, 2021. 182:106699.
<https://doi.org/10.1016/j.jcsr.2021.106699>.
- [6] Jelle, B.P. Accelerated climate ageing of building materials, components and structures in the laboratory. *J Mater Sci* **47**, 6475–6496 (2012). <https://doi.org/10.1007/s10853-012-6349-7>
- [7] Castro, J.M., Araújo, M., D’Aniello, M., Landolfo, R. (2018). Strengthening of RC Buildings with Steel Elements. In: Costa, A., Arêde, A., Varum, H. (eds) *Strengthening and Retrofitting of Existing Structures. Building Pathology and Rehabilitation*, vol 9. Springer, Singapore. https://doi.org/10.1007/978-981-10-5858-5_6
- [8] Monika Z., Joanna M. Analysis of Historic Brick Walls’ Strengthening Methods[J]. *Procedia Engineering*, 2016, 161:771-776. <https://doi.org/10.1016/j.proeng.2016.08.702>.
- [9] Ahmed H., Ramy I. S., Mizan A., Aref A. A., Abedulgader B., Saad A. Y., Strengthening of reinforced concrete columns incorporating different configurations of stainless-steel plates[J]. *Structures*, 2024. 64:106577. <https://doi.org/10.1016/j.istruc.2024.106577>.
- [10] Zhu H, Chen H, Fu Z, Guo Z, Liu P, Chen Y. Experimental Study on Axial Compressive Load-Bearing Performance of RC Short Columns Strengthened by All-Light Ceramsite Concrete. *Applied Sciences*. 2022; 12(21):11206. <https://doi.org/10.3390/app122111206>.
- [11] Habib, A., Yildirim, U. & Eren, O. Column repair and strengthening using RC jacketing: a brief state-of-the-art review. *Innov. Infrastruct. Solut.* **5**, 75 (2020). <https://doi.org/10.1007/s41062-020-00329-4>.
- [12] Zhong, S., Hu, X., Peng, G. *et al.* The Effect of Section Enlargement with Cementitious Grout on the Eccentric Compression Behavior of RC Columns. *KSCE J Civ Eng* 2024. **28**: 3378–3393.
<https://doi.org/10.1007/s12205-024-1211-4>.
- [13] Deng M., Zhang Y., Chen S. Experimental research of the seismic performance of frame columns strengthened with high ductile concrete jacket and analysis of the limitation of axial load ratio[J]. *China Civil Engineering Journal*, 2019. 52(2):22-65. 10.15951/j.tmgcxb.2019.02.003.
- [14] Joaquín G., Antoni C., Francisco J., Pedro A., Jose M. Joint strengthening by external bars on RC beam-column joints[J]. *Journal of Building Engineering*, 2022. 45:103445.
<https://doi.org/10.1016/j.jobe.2021.103445>.
- [15] Praveen A, Ajay K S. Effect of reinforced concrete jacketing on axial load capacity of reinforced concrete column[J]. *Civil Engineering Journal*, 2020, (7): 1266-1272.
- [16] ACI 318-14. ACI Committee 318. *Building code requirements for structural concrete and commentary*[S]. American Concrete Institute, Farmington Hills; 2014.
- [17] Rawaa S., Alaa H. Behavior of RC columns strengthened by combined (CFRP and steel jacket) [J] *Materials*

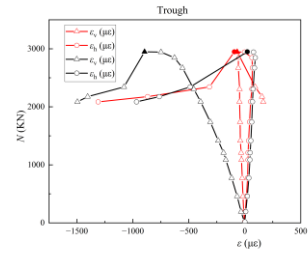
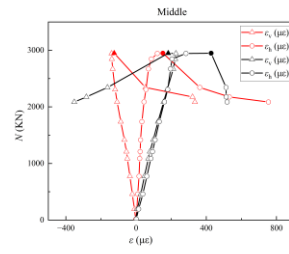
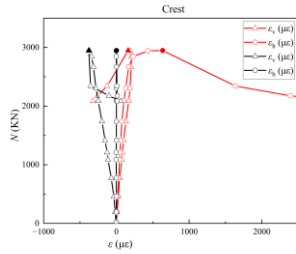
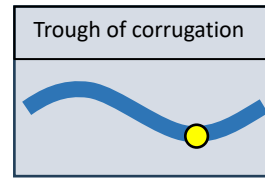
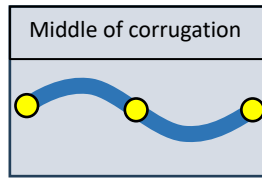
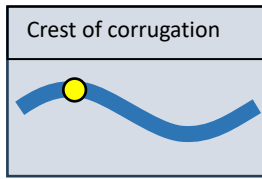
- Today: Proceedings, 2022. 61:1126-1134. <https://doi.org/10.1016/j.matpr.2021.10.514>.
- [18] Tarabia A.M. , Albakry H.F. Strengthening of RC columns by steel angles and strips[J]. Alexandria Engineering Journal, 2014. 53(3):615-626. <https://doi.org/10.1016/j.aej.2014.04.005>.
- [19] Wang, L.; Su, R.K.L.; Cheng, B.; Li, L.Z.; Wan, L.; Shan, Z.W. Seismic behavior of preloaded rectangular RC columns strengthened with precambered steel plates under high axial load ratios. *Eng. Struct.* **2017**, *152*, 683–697.
- [20] Fakharifarah, M.; Chen, G.D.; Wu, C.L.; Shamsabadi, A.; ElGawady, M.A.; Dalvand, A. Rapid repair of earthquake-damaged RC columns with prestressed steel jackets. *J. Bridge Eng.* **2016**, *21*.
- [21] Choi, E.; Chung, Y.S.; Park, C.; Kim, D.J. Seismic performance of circular RC columns retrofitted with prefabricated steel wrapping jackets. *Mag. Concr. Res.* **2013**, *65*, 1429–1440. <https://doi.org/10.1680/macrcr.13.00177>.
- [22] Zeng C., Chen Z., Deng Z., Yang Z. Tests and analysis of HSC-filled steel tube columns strengthened by CFRP and angle steel frame under eccentric compression[J]. Structures, 2025. 71. <https://doi.org/10.1016/j.istruc.2024.108111>.
- [23] Zhang, S., Miao, K., Wei, Y. *et al.* Experimental and Theoretical Study of Concrete-Filled Steel Tube Columns Strengthened by FRP/Steel Strips Under Axial Compression. *Int J Concr Struct Mater* **17**, 1 (2023). <https://doi.org/10.1186/s40069-022-00556-2>
- [24] Pendhari S S, Kant T, Desai Y M. Application of polymer composites in civil construction: A general review[J]. Composite Structures, 2008, 84(2): 114-124.
- [25] Tarabia A M, Albakry H F. Strengthening of RC columns by steel angles and strips[J]. Alexandria Engineering Journal, 2014, 53(3): 615-626.
- [26] Moshiri N, Hosseini A, Mostofinejad D. Strengthening of RC columns by longitudinal CFRP sheets: Effect of strengthening technique[J]. Construction and Building Materials, 2015, 79: 318-325.
- [27] Frangou M, Pilakoutas K, Dritsos S. Structural repair/strengthening of RC columns[J]. Construction and Building Materials, 1995, 9(5): 259-266.
- [28] Raza S, Khan M K I, Menegon S J, et al. Strengthening and Repair of Reinforced Concrete Columns by Jacketing: State-of-the-Art Review[J]. Sustainability, 2019, 11(11): 3208.
- [29] Islam N, Hoque M M. Strengthening of Reinforced Concrete Columns by Steel Jacketing: A State of Review[J]. [no date], 05(03). .
- [30] Shang X, Yu J, Li L, et al. Strengthening of RC Structures by Using Engineered Cementitious Composites: A Review[J]. Sustainability, 2019, 11(12): 3384.
- [31] Kaish A B M A, Jamil M, Raman S N, et al. Ferrocement composites for strengthening of concrete columns: A review[J]. Construction and Building Materials, 2018, 160: 326-340.
- [32] Ghobarah A, Biddah A, Mahgoub M. Rehabilitation of reinforced concrete columns using corrugated steel jacketing [J]. Journal of Earthquake Engineering, 1997, 1(4): 651-673.
- [33] Biddah A, Ghobarah A, Aziz T S. Upgrading of Nonductile Reinforced Concrete Frame Connections[J]. Journal of Structural Engineering, 1997, 123(8): 1001-1010.
- [34] Tomii M, Sakino K, Xiao Y, et., al. Earthquake resisting hysteretic behavior of reinforced concrete short columns confined by steel tube[C]//Proceedings of the international speciality conference on concrete filled steel tubular structures, Harbin, China. 1985: 119-25.
- [35] Yang L, Wang Y, Elchalakani M, et al. Experimental behavior of concrete-filled corrugated steel tubular short columns under eccentric compression and non-uniform confinement[J]. engineering structures, 2020, 220: 111009.
- [36] Wang Y., Yang L., Yang H. and Liu C. Behaviour of concrete-filled corrugated steel tubes under axial

- compression [J]. *Engineering Structures*, 2019, 183: 475-495.
- [37] Ault J P, Elzly P E. Durability of Aluminized Type 2 Coated Corrugated Steel Pipe Exposed Throughout the United States[R]. Washington, D.C.: National Corrugated Steel Pipe Association, 2014.
- [38] Fang Y, Liu C, Yang H, et al. Axial behaviour of concrete-filled corrugated steel tubular column embedded with structural steel[J]. *Journal of Constructional Steel Research*, 2020, 170: 106064.
- [39] Fang Y, Wang Y, Hou C, et al. CFDST stub columns with galvanized corrugated steel tubes: Concept and axial behaviour[J]. *thin-walled structures*, 2020, 157: 107116.
- [40] Zou Y, Wang L, Sun Z, et al. Experimental and numerical studies of concrete-filled corrugated steel tubular column under axial compression[J]. *Engineering Structures*, 2023, 276: 114813.
- [41] Yu C-Q, Tong G-S, Duan S-J, et al. Combined axial and flexural behavior of concrete-filled corrugated steel tubular columns[J]. *Journal of Constructional Steel Research*, 2024, 221: 108912.
- [42] Nassirnia M, Heidarpour A, Zhao X-L, et al. Innovative hollow columns comprising corrugated plates and ultra high-strength steel tubes[J]. *Thin-Walled Structures*, 2016, 101: 14-25.
- [43] Lu B., Fang Y., Wang Y., Yang H., Li H. Experimental behaviour of concrete-filled double-skin corrugated steel tubes under combined compression and cyclic lateral loads [J]. *Engineering Structures*, 2025. 327:119545. <https://doi.org/10.1016/j.engstruct.2024.119545>.
- [44] Handousa, A.M., Abdellatif, M., Salem, F.A. *et al.* Experimental and analytical study on axial behaviour of square corrugated concrete filled single and double skin tube stub columns. *Sci Rep* **15**, 2167 (2025). <https://doi.org/10.1038/s41598-025-85585-z>.
- [45] Jin Z., Xie F., Yang T., Han X., Chen X., Zhang Y. Fractal dimension analysis of concrete specimens under different strain rates[J]. *Journal of Building Engineering*, 2023, 76:107044
- [46] GB/T 228.1-2010, Metallic materials - Tensile testing - Part 1: Method of test at ambient temperature[S]. Standardization Administration of the People's Republic of China, Beijing, China. ISO 6892-1:2009, MOD [in Chinese]
- [47] GB/T 1499.2-2018. Steel for concrete reinforcement - Part 2: Hot-rolled ribbed steel bars[S]. Standardization Administration of the People's Republic of China, Beijing, China. ISO 6935-2:2015. [in Chinese]
- [48] ASTM A370-17a. Standard Test Methods and Definitions for Mechanical Testing of Steel Products (ASTM A370-17a)[S]. ASTM International, West Conshohocken, PA, USA, 2017. <https://doi.org/10.1520/A0370-17A>
- [49] GB/T50081-2019. Standard for test methods of concrete physical and mechanical properties[S]. China Architecture & Building Press, Beijing, China, 2019. [in Chinese]
- [50] GB50488-2015. Technical code for application of cementitious grout[S]. China Architecture & Building Press, 2015. [in Chinese]
- [51] GB/T 17671-2021. Test method of cement mortar strength (ISO method) [S]. Standards Press of China, Beijing, China, 2021. ISO 679:2009. [in Chinese]
- [52] Han L.H. Tests on stub columns of concrete-filled RHS sections[J]. *Constr Steel Res* 2002, 58: 353-372.
- [53] Feng P., Qiang H., Ye L. Discussion and definition on yield points of materials, member and structures[J]. *Engineering Mechanics*, 2017, 34(3): 36-46. doi: 10.6052/j.issn.1000-4750.2016.03.0192.
- [54] Ouyang Y., Kwan A.K.H. Finite element analysis of square concrete-filled steel tube (CFST) columns under axial compressive load [J]. *Engineering Structures* 2018, 156:443-459. <https://doi.org/10.1016/j.engstruct.2017.11.055>.
- [55] Ma W., Yan Y., Lu Y., Li S., Wang L. Axially loaded square CFST short columns strengthened with high-strength square steel tubes and concrete jackets[J]. *Engineering Structures*, 2025. 324:119395. <https://doi.org/10.1016/j.engstruct.2024.119395>.
- [56] Yu M, Zha X, Ye J, et al. A unified formulation for circle and polygon concrete-filled steel tube columns under

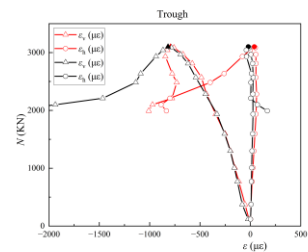
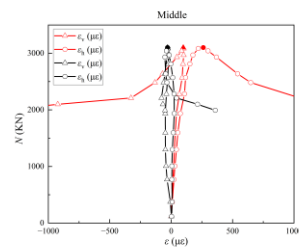
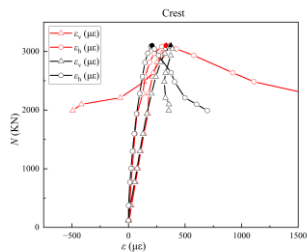
- axial compression[J]. *Engineering Structures*, 2013, 49: 1-10. <https://doi.org/10.1016/j.engstruct.2012.10.018>
- [57] Li X, Liao X, Li Z-Y, et al. Confinement mechanism of rectangular CFST components using double horizontally-corrugated steel plates[J]. *Structures*, 2023, 57: 105107. <https://doi.org/10.1016/j.istruc.2023.105107>
- [58] Chakrabarty J. *Theory of plasticity*[M]. 3rd ed. UK: Elsevier Butterworth-Heinemann, 2005.
- [59] Park R, Priestley M, et al. Ductility of square confined concrete columns[J]. *Journal of Structural Engineering*, 1982, 108(4): 929–950.
- [60] Hoang A L and Ekkehard F. Numerical study of circular steel tube confined concrete (STCC) stub columns - ScienceDirect[J]. *Journal of Constructional Steel Research*, 2017, 136: 238-255.
- [61] Richart E. *A Study of the Failure of Concrete under Combined Compressive Stresses*[J]. Bulletin: University of Illinois, Engineering Experimental Station, 1928.
- [62] CEN. Eurocode 2: design of concrete structures – Part 1-1: General rules and rules for buildings. NEN-EN 1992-1-1:2005. Brussels, Belgium: Comité Européen de Normalisation; 2005.
- [63] Xuhong Zhou, Jiepeng Liu, Xuanding Wang, Pengfei Liu, Kwok-Fai Chung, Wei Wei. Structural Performance and Compression Resistances of Thin-Walled Square CFST Columns with Steel Lining Tubes[J]. *Journal of Structural Engineering* 2021, 147(7). [https://doi.org/10.1061/\(ASCE\)ST.1943-541X.0003069](https://doi.org/10.1061/(ASCE)ST.1943-541X.0003069)
- [64] Candappa D C, Sanjayan J G, Setunge S. Complete triaxial stress–strain curves of high-strength concrete[J]. *Journal of Materials in Civil Engineering*, 2001, 13(3): 209–215.
- [65] Saatcioglu M and Razvi S R. Strength and ductility of confined concrete[J]. *Journal of Structural Engineering*, 1992, 118(6): 1590-1607.
- [66] Hoshikuma J, Kawashima K, Nagaya K, Taylor AW. Stress-strain model for confined reinforced concrete in bridge piers[J]. *Journal of Structural Engineering*, 1997, 123(5): 624–633.
- [67] Fafitis A and Shah S. Predictions of ultimate behavior of confined columns subjected to large deformations [J]. *ACI Structural Journal*, 1985, 82(4): 423–433.
- [68] Mander J B, Priestley M J N. Theoretical Stress-Strain Model for Confined Concrete[J]. *Journal of Structural Engineering*, 1988, 114(8): 1804-1826.
- [69] Attard M. Stress-Strain Relationship of Confined and Unconfined Concrete [J]. *ACI Materials Journal*, 1996, 93(5): 432-442.
- [70] Setunge S, Attard M, Darvall P. Ultimate strength of confined very high-strength concretes[J]. *ACI Structural Journal*, 1993, 90(6):632-641.
- [71] Cusson D, and Paultre P. Stress-strain model for confined high strength concrete[J]. *Journal of Structural Engineering*, 1995, 121(3): 468-477.
- [72] Legeron F and Paultre P. Uniaxial confinement for normal and high-strength concrete columns[J]. *Journal of Structural Engineering*, 2003, 129(2): 241-252.
- [73] Bousalem B and Chikh N. Development of a confined model for rectangular ordinary reinforced concrete columns[J]. *Materials and Structures*, 2007, 40: 605–606.
- [74] Girgin Z C, Arioglu N, Arioglu E. Evaluation of strength criteria for very-high-strength concretes under triaxial compression[J]. *ACI Structural Journal*, 2007, 104 (S27): 277-283.
- [75] Megahed, K., Mahmoud, N.S. & Abd-Rabou, S.E.M. Finite Element Modeling for Concrete-Filled Steel Tube Stub Columns Under Axial Compression. *Int J Steel Struct* 24, 1229–1250 (2024). <https://doi.org/10.1007/s13296-024-00896-7>.
- [76] Lim J C and Ozbakkaloglu T. Stress-strain model for normal- and light-weight concretes under uniaxial and triaxial compression[J]. *Construction and Building Materials*, 2014, 71: 492–509.
- [77] Fang Y, Wang Y, Elchalakani M, et al. Experimental investigation on concrete-filled corrugated steel tubular

- column under constant axial load and cyclic load[J]. *Engineering Structures*, 2021, 248: 113245.
- [78] Fang Y., Wang Y., Yang L. and Yang H. Uniaxial Monotonic and Cyclic Compressive Stress–Strain Model for Concrete-Filled Thin-Walled Helical Corrugated Steel Tubes[J]. *Journal of Structural Engineering* 2023, 149(6): <https://doi.org/10.1061/JSENDH.STENG-11719>
- [79] Jiepeng Liu, Xuanding Wang, Sumei Zhang. Behavior of square tubed reinforced-concrete short columns subjected to eccentric compression[J]. *Thin-Walled Structures* 2015, 91:108-115. <https://doi.org/10.1016/j.tws.2015.01.023>.

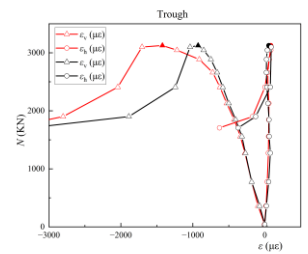
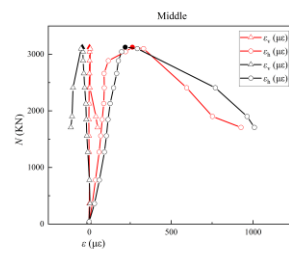
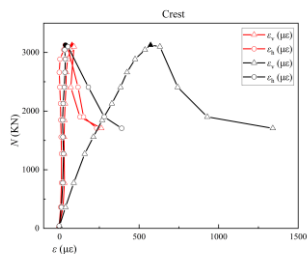
Appendix



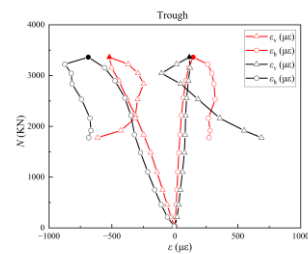
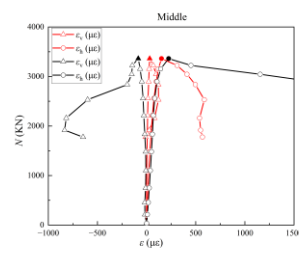
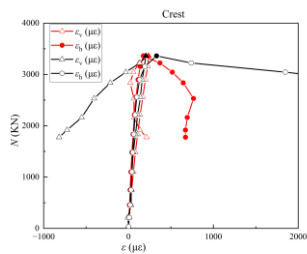
Load-strain curves of CS-A-2-20-0.4



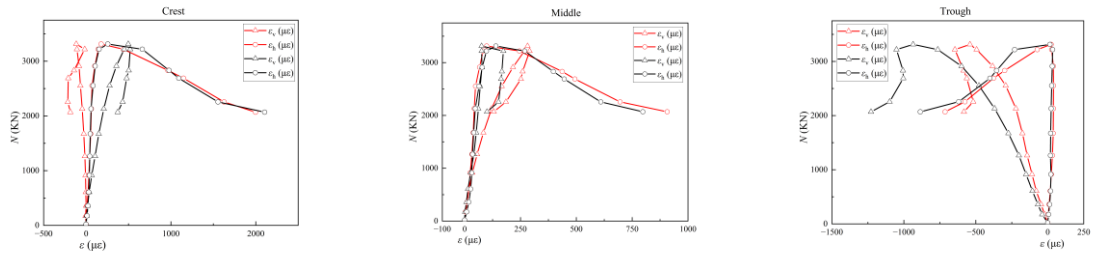
Load-strain curves of CS-B-2-20-0.4



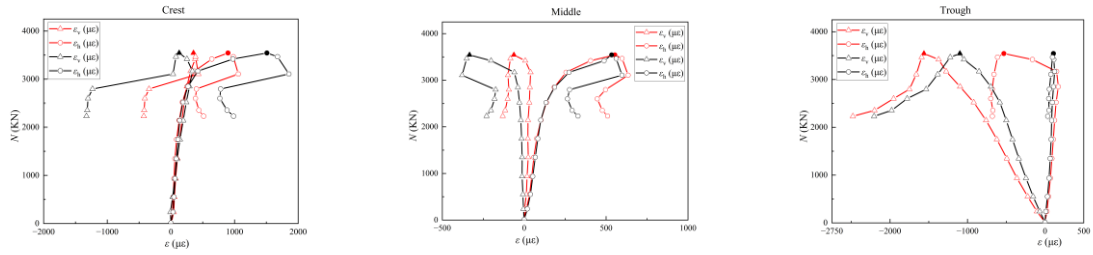
Load-strain curves of CS-C-2-20-0.4



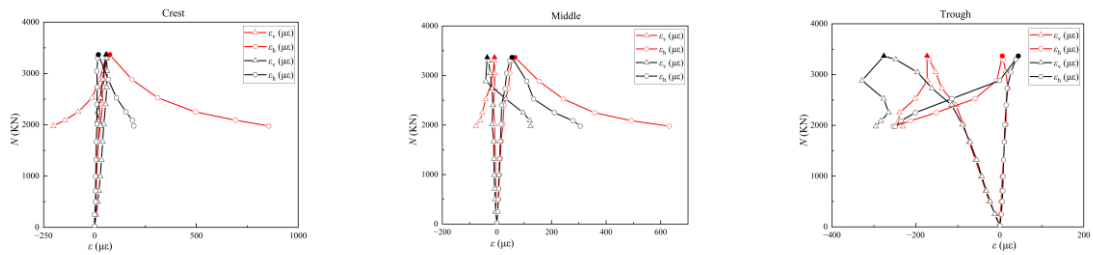
Load-strain curves of CS-D-1.6-20-0.4



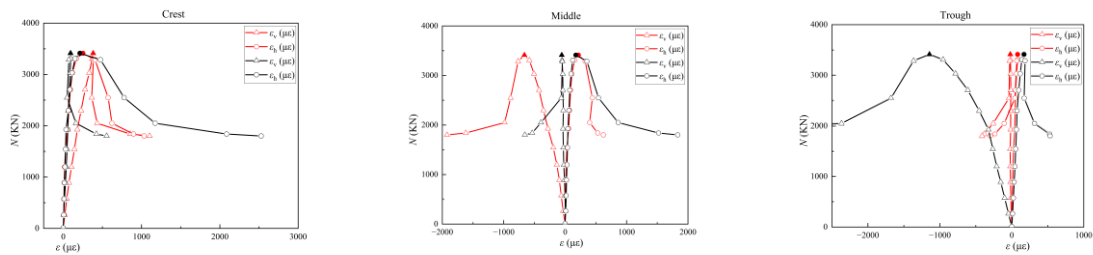
Load-strain curves of CS-D-2.7-20-0.4



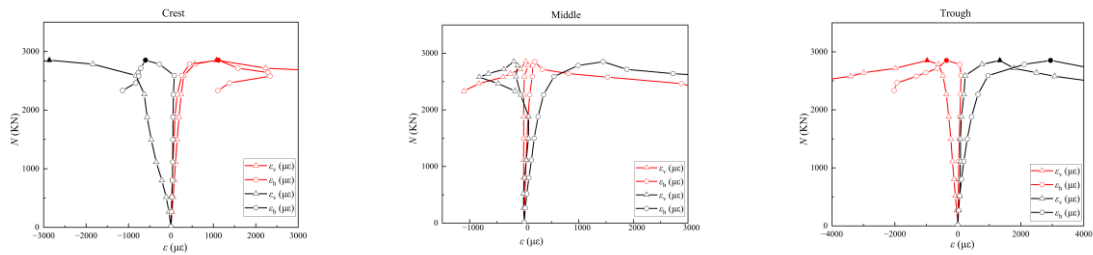
Load-strain curves of Load-strain curves of CS-D-2-20-0.4



Load-strain curves of CS-D-2-20-0.6-a



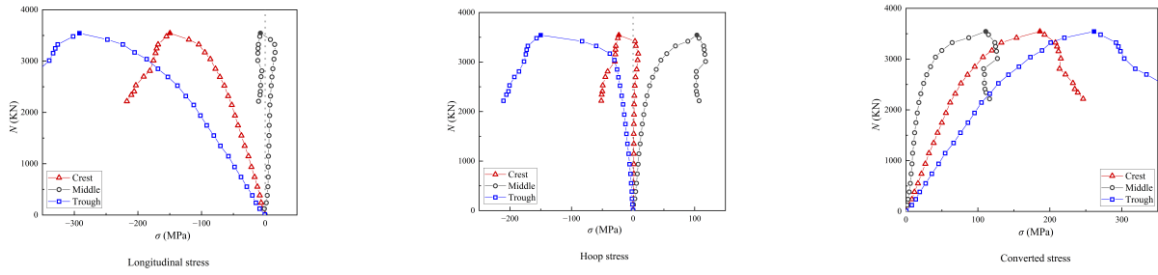
Load-strain curves of CS-D-2-20-0.6-b



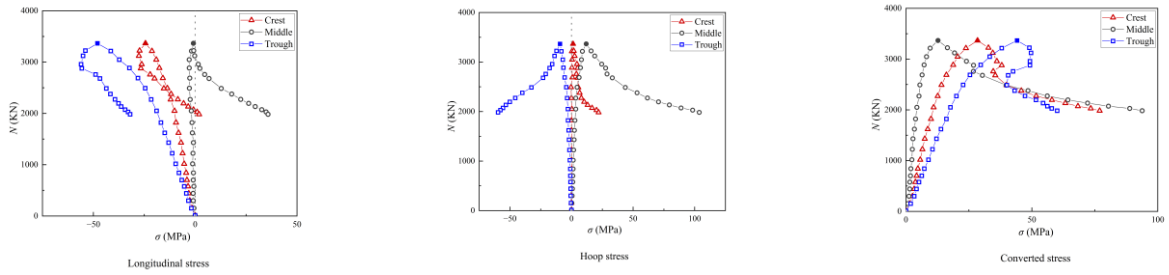
Load-strain curves of CS-D-2-20-1

Fig. A-1. Strain components development in corrugated steel.

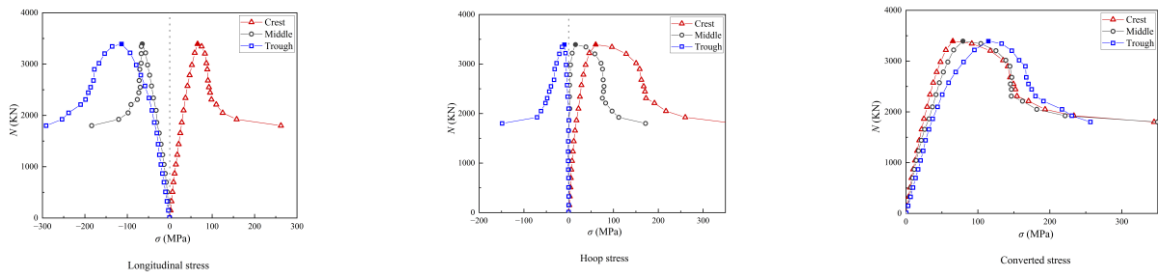
Load-stress curves of CS-D-2.7-20-0.4



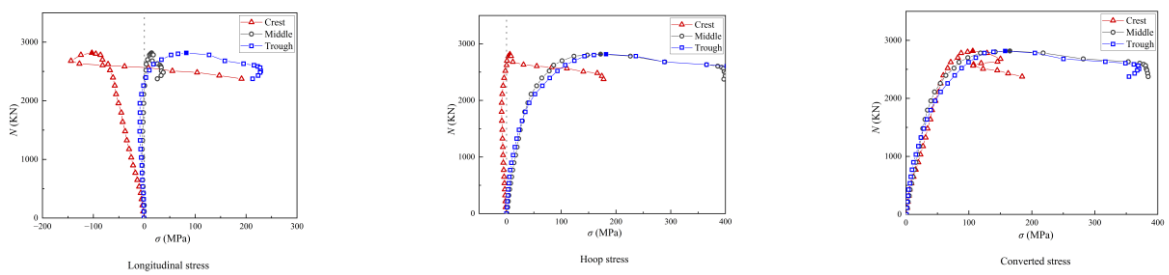
Load-stress curves of CS-D-2-20-0.4



Load-stress curves of CS-D-2-20-0.6-a



Load-stress curves of CS-D-2-20-0.6-b



Load-stress curves of CS-D-2-20-1

Fig. A-2. Strain components development in corrugated steel jacket.